Am J Cancer Res 2019;9(2):390-405
www.ajcr.us /ISSN:2156-6976/ajcr0089170

Original Article

Inhibition of invasive pancreatic cancer: restoring cell apoptosis by activating mitochondrial p53

Jiongjia Cheng[1], Karl J Okolotowicz[1], Daniel Ryan[1], Evangeline Mose[2], Andrew M Lowy[2], John R Cashman[1]

[1]Human BioMolecular Research Institute and ChemRegen, Inc., San Diego, CA 92121, USA; [2]Department of Surgery, Division of Surgical Oncology, University of California at San Diego, Moores Cancer Center, La Jolla, CA 92093, USA

Received November 29, 2018; Accepted December 6, 2018; Epub February 1, 2019; Published February 15, 2019

Abstract: Pancreatic ductal adenocarcinoma (PDAC), constitutes >90% of pancreatic cancers (PC) and is one of the most aggressive human tumors. Standard chemotherapies for PDAC (e.g., gemcitabine, FOLFIRINOX, etc.) has proven to be largely ineffective. Herein, we report a novel molecule (i.e., compound **1**) that potently inhibits proliferation and induces apoptosis of PDAC cells. As we observed in other cancer types (i.e., colorectal, breast cancer), the effect of **1** against PDAC cells is also related to microtubule destabilization and DNA damage checkpoint activation. However, in PDAC cells, the inhibitory effect of **1** was mainly controlled by mitochondrial p53-dependent apoptosis. Compound **1** worked with cells of different p53 mutant status and affected p53 activation/phosphorylation not simply by stabilizing p53 protein but through antagonizing anti-apoptotic effects of Bcl-xL and restoring p53 to activate mitochondrial-apoptotic pathways (i.e., cytochrome c release, caspase activation and PARP cleavage). Compound **1** was more efficient than a typical PDAC combination therapy (i.e., gemcitabine with paclitaxel) and showed synergism in inhibiting PDAC cell proliferation with gemcitabine (or gemcitabine with paclitaxel). This synergism varied between different types of PDAC cells and was partially controlled by the phosphorylation of p53 on Serine15 (phospho-Ser15-p53). In vivo studies in an orthotopic syngeneic murine model showed that **1** (20 mg/kg/day, 28 days, i.p.) inhibited tumor growth by 65% compared to vehicle-treated mice. No apparent acute or chronic toxicity was observed. Thus, compound **1** utilizes a distinct mechanism of action to inhibit PC growth in vitro and in vivo and is a novel anti-PDAC compound.

Keywords: Pancreatic cancer, pancreatic ductal adenocarcinoma (PDAC), p53 activation, mitochondrial control of apoptosis, DNA damage pathway, orthotopic syngeneic model

Introduction

In the United States, pancreatic cancer (PC) is the third leading cause of cancer-related fatalities and will result in an estimated 44,330 deaths during 2018 [1]. It has been projected that PC will become the second most prevalent cause of cancer-related death by 2030 [2]. Pancreatic ductal adenocarcinoma (PDAC) is the most common form of PC [1]. Despite its prevalence, therapeutic options for PDAC are limited to surgery and/or combination of chemotherapy and radiotherapy. Due to drug resistance and drug-induced side effects, first-line chemotherapy (i.e., gemcitabine, 5-fluorouracil or FOLFIRINOX, etc.) have made minimal impact on PDAC treatment [3-6]. While treatment of mutant resistant PDAC tumors with combination therapies (e.g., gemcitabine with nab-paclitaxel) show improvement over single agent therapies [7, 8], they are highly toxic [9]. Thus, there is a major unmet medical need to develop selective and effective treatments to sensitize and drive PDAC cells towards cell death without harming normal cells.

Therapies targeting protein components of dysregulated signal transduction pathways can be efficacious anti-cancer therapies with minimal adverse effects [10]. The pathogenesis of cancer is characterized by clinically relevant genetic alterations leading to either activation of

oncogenes or inactivation of tumor suppressor genes [11, 12] (e.g., inactivation of p53 function). As previously reported, compound **1** (**Figure 1A**) decreased cellular proliferation and induced apoptosis in several cancer cells (i.e., colon and breast cancer) [13-15]. **1** is a non-toxic DNA damage pathway inhibitor that suppresses cancer cell growth and survival [13-15] and is distinct from classic DNA damage agents that often cause significant toxicity [16]. Tumor suppressor protein p53 plays a critical role in cellular response to DNA damage and other genomic aberrations, and is an attractive target for mechanism-driven anti-cancer drug discovery [11, 17].

Accumulation of p53 in cytoplasmic and nuclear fractions in response to DNA damage works via multiple pathways to induce cell apoptosis. After p53 stabilization, p53 accumulation in the nucleus directly regulates the expression of pro-apoptotic genes (i.e., Bax, Bak, etc.). Extranuclear p53 apoptotic cell death mechanisms are dependent on transactivation-deficient p53 localization to cytosol or mitochondria-associated membrane and/or endoplasmic reticulum (ER) [18-20]. In mitochondrial-controlled cell apoptosis (intrinsic pathway), trafficking of mitochondria-bound Bcl-2 family members (i.e., Bax, Bad, Bak, etc.) cause the release of mitochondrial cytochrome c into cytosol, where it binds to adaptor proteins leading to activation of "executioner" caspases (i.e., caspase-3, -6 or -7) and Poly (ADP-ribose) polymerase (PARP) cleavage [21, 22]. Approximately 75% of PDAC's harbor intragenic p53 mutations [6, 23]. Mutant versions of p53 make PDAC cells resistant to chemotherapeutic regimens [23] due to loss of functional effects activated by p53 (i.e., growth arrest, apoptosis and senescence). An over-arching challenge is to develop a drug that potently inhibits PDAC growth by restoring tumor suppressor function.

Herein, we report that **1** potently decreased PDAC cell proliferation by activating DNA damage checkpoint and apoptotic pathways (e.g., the mitochondrial (intrinsic) control of apoptosis). In the presence of **1**, gemcitabine (or gemcitabine with paclitaxel) showed enhanced/synergistic potency to inhibit proliferation of several types of PDAC cells. In a syngeneic, orthotopic model of PDAC, **1** inhibited tumor growth without any apparent acute or chronic toxicity. **1** was non-toxic and possessed attractive pharmaceutical and pharmacological properties. **1** is capable of simultaneously targeting the key pro-survival pathway(s) implicated in PDAC. Accordingly, **1** is a unique and attractive small molecule as a novel PDAC therapy.

Materials and methods

Cell lines

MIA PaCa-2 (CRL-1420), HPAC (CRL-2199), AsPC-1 (CRL-1682) and BxPC-3 (CRL-1687) PDAC cell lines were purchased from American Type Culture Collection (ATCC). LM-P, 779E and 1334E cell lines were obtained from Dr. Andrew Lowy (UC San Diego, CA). LM-P cells were isolated from liver of $Kras^{G12D/+}$; LSL-$Trp53^{R172H/+}$; Pdx-1Cre mice [24, 25] and 779E and 1334E were two patient-derived, low passage primary PDAC cell lines [26]. Commercial cell lines were grown according to ATCC recommendations and authenticated by short tandem repeat (STR) DNA profiling at ATCC. LM-P, 779E and 1334E cells were characterized and cultured as reported [24-26]. After thawing, cell lines (within 10 passages; less than 6 weeks) were cultured at 37°C in a humidified 5% CO_2 atmosphere and screened for Mycoplasma using MycoAlert PLUS Mycoplasma Detection Kit (Lonza).

Cell proliferation and apoptosis

PDAC cells were seeded and treated with vehicle (0.5% DMSO), or **1** (1.6-5000 nmol/L, 16-72 hours). Cell proliferation was determined by SYBR green (cellular DNA detection) fluorescence intensity (Ex_{495} nm, Em_{535} nm) measurement [13]. A similar protocol was used to test the synergistic effect of **1** in the presence of gemcitabine and/or paclitaxel. Chou-Talalay analysis used commercial software (ComboSyn) [27]. Cell apoptosis was determined by a caspase-3/7 assay with a Caspase-Glo 3/7 Assay (Promega) [13].

Subcellular fractionation and immunoblots

PDAC cells were seeded and treated with vehicle or **1** (i.e., 1.6-5000 nmol/L, 2-32 hours).

Whole-cell extracts were obtained by lysis with RIPA buffer and centrifugation at 14,000 × g. For subcellular fractionation, 2×10^7 cells were suspended in isolation buffer (225 mmol/L mannitol, 75 mmol/L sucrose, 50 mmol/L HEPEs pH 7.5 with 1 × protease inhibitors) [28] and homogenized at 4°C. The nuclear fraction was isolated from cell suspensions from the pellet after centrifugation at 600 × g. The supernatant was collected for further separation of a mitochondrial fraction (pellet) and cytosolic fraction (supernatant) by centrifugation at 7,000 × g. The pellets (i.e., nuclear or mitochondrial fractions) were washed, suspended in RIPA buffer and sonicated to fully extract nuclear or mitochondrial proteins. Protein extracts were resolved by SDS-PAGE followed by Western blotting using antibodies specific for target proteins (Supplementary Materials and Methods). Densities of the Western blot bands were quantified using ImageJ (NIH).

Immunoprecipitation

Protein A agarose beads pre-cleaned with control rabbit IgG were used with rabbit Bcl-xL IgG pull-down (Cell Signaling). Beads with sequestered antibody were added to cytosolic extracts of MIA PaCa-2 and BxPC-3 cells and incubated with gentle mixing (4 hours at 4°C) and pelleted by centrifugation at 2,000 × g for 30 sec at 4°C. Eluted protein was resolved by SDS-PAGE followed by Western blotting.

Immunofluorescence analysis of mitochondrial structure and cytochrome c distribution

Cells grown on glass coverslips were treated with vehicle, **1** (i.e., 50 nmol/L), a combination of gemcitabine (i.e., 50 nmol/L) and paclitaxel (i.e., 5 nmol/L), or staurosporine (i.e., 1 μmol/L) for 24 hours. Fifteen min prior to the end of treatment, live cells were incubated with MitoTracker-Red-CMXRos (Thermo Fisher Sci.) to label mitochondria. Cells were fixed in 3.7% paraformaldehyde followed by permeabilization in 0.1% saponin. After washing in PBS, cells were blocked in 4% bovine serum albumin for 1 hour at r.t. and then incubated with anti-cytochrome c antibody (1:200) overnight at 4°C. Finally, cells were incubated with Alexa Fluro 488-conjugated goat anti-mouse IgG (1:1000) for 1 hour at r.t. Coverslips were mounted on slides using Prolong Gold Antifade Mountant (Life Technologies) and observed under a Zeiss LSM 880 airyscan confocal microscope with 63 × oil immersion objective. Images were analyzed with Image J.

Orthotopic PDAC murine model

Log-phase LM-P cells were harvested and resuspended in basement membrane-Matrigel Matrix (Corning). Animal work was conducted in accordance with the Guide for Care and Use of Laboratory Animals as adopted by the NIH. Formal approval was obtained from the IACUC of HBRI. 7-week-old female B6129SF1/J mice (Jackson Laboratory) were anesthetized for surgery. Under anesthesia, 3.5×10^5 LM-P cells in 20 μL Matrigel was injected into the pancreas. Five days after tumor cell inoculation, mice were dosed daily (i.p., 28 days) with vehicle (aqueous-DMSO-Captisol, n=7), low dose (10 mg/kg/day, n=6) or high dose (20 mg/kg/day, n=7) of **1**. At day 32, mice were killed and tumors excised for immunoblot and qPCR analysis of protein markers (i.e., p53) and histological analysis of H&E (tissue morphology) and TUNEL (apoptosis). Tumor volume was calculated based on the formula for ellipsoid volume, $V=4/3 \times \pi \times (W/2)(L/2)(H/2)$, where W, L, H are width, length, and height in millimeters, respectively. Blood samples were collected [29] and serum was separated by centrifugation for analysis of markers of liver and kidney function (IDEXX Laboratories).

Quantitative real-time PCR

Total RNA was extracted from PDAC cells treated with vehicle, **1** or colchicine (i.e., 500 nmol/L, 4 hour) or the tumor tissue (1 mg) using Trizol (Life Technologies). cDNA was made using 500 ng of total RNA with an iScript kit (Bio-Rad). qPCR incubations were run with 200 nmol/L of gene-specific primers (Table S1) and SYBR Green qPCR Master Mix (Bio-Rad). qPCR data was analyzed by the ΔΔCt method [30].

Statistical analysis

IC_{50} and EC_{50} values were calculated using a nonlinear regression analysis (GraphPad Prism,

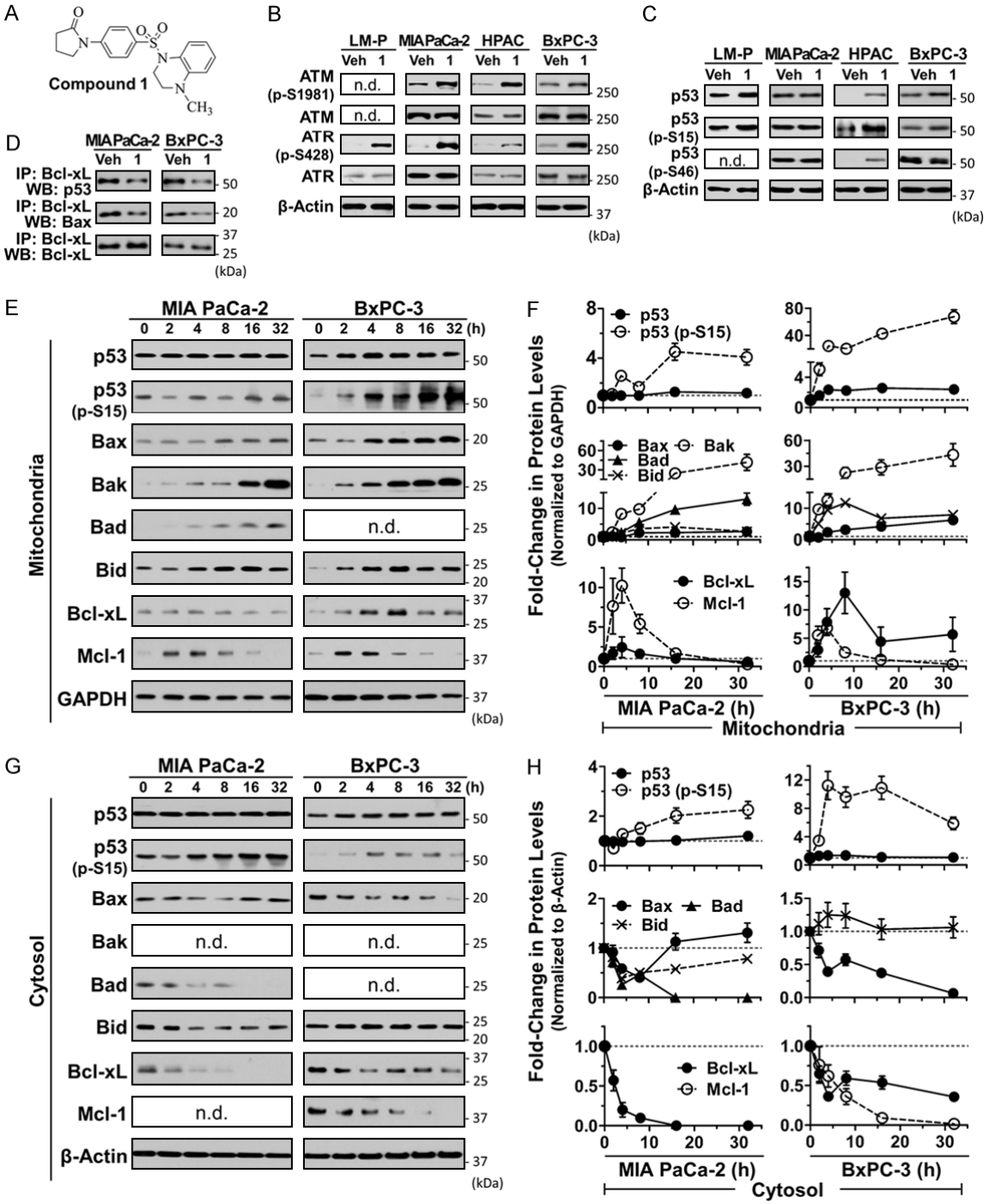

Figure 1. (A) Structure of compound **1**. (B-D) effect of **1** on activation of DNA damage checkpoints and p53, (E-H) cellular trafficking and translocation of pro-apoptotic and anti-apoptotic markers as a function of time (0 to 32 hours). Western blot analysis of **1** on (B) phospho(Ser1981)-ATM, total ATM, phospho(Ser428)-ATR, total ATR and (C) total p53, phospho(Ser15)-p53, phospho(Ser46)-p53 as determined from whole-cell extracts of LM-P, MIA PaCa-2, HPAC and BxPC-3 cells following 4 hours treatment with **1**. (D) Effect of **1** on the interaction of p53 or Bax with Bcl-xL by immunoprecipitation in cytosolic extracts of MIA PaCa-2 or BxPC-3 cells. (E-H) Western blot and densitometry analysis of effects of **1** on p53, phospho(Ser15)-p53, Bax, Bak, Bad, Bid, Bcl-xL and Mcl-1 as determined from mitochondrial (E, F) and cytosolic (G, H) extracts of MIA PaCa-2 and BxPC-3 cells. The concentration of **1** was 40 nmol/L in (B and C), 50 nmol/L in (D, E and G); Veh, vehicle control (0.5% DMSO). A total of 25 μg of whole-cell extracted protein (B, C) and 10 μg of subcellular extracted protein (E, G) was loaded into each lane. GAPDH was used as a mitochondrial

internal control and β-actin was used as an internal control of cytosolic and whole-cell extracts. Data are mean ± SD (n=3) in (F and H); n.d., not detected.

Table 1. Effect of compound **1** on PDAC cell proliferation and apoptosis

Cell Lines	Anti-Proliferation IC_{50} ± SD, nmol/L (*N*)[a]	Apoptosis EC_{50} ± SD, nmol/L (*N*)[a]	p53 status (References)
LM-P	15 ± 3 (*3*)	3.5 ± 1.4 (*3*)	Arg172His [24, 25]
MIAPaCa-2	12 ± 2 (*3*)	16 ± 2 (*3*)	Arg248Trp [46]
HPAC	12 ± 5 (*4*)	14 ± 5 (*4*)	Wild-Type [46]
BxPC-3	13 ± 7 (*4*)	12 ± 2 (*4*)	Tyr220Cys [48]
AsPC-1	13 ± 6 (*4*)	>5000[b]	135Δ1bp, $^{-/-}$p53 [31]
779E	9.8 ± 2.0 (*3*)	>5000[b]	Arg209Lys, $^{-/-}$p53 [26][c]
1334E	8.7 ± 1.7 (*3*)	11 ± 6 (*3*)	Arg175His [26]

[a]IC_{50} or EC_{50} is the mean ± the standard deviation (SD) of 3-4 independent determinations. *N* stands for the number of replicate experiments. [b]Compound **1** was not potent up to 5000 nmol/L treatment in AsPC-1 and 779E cells. [c]Codon 210 - insertion of A and codon 215 - premature stop (like $^{-/-}$p53).

San Diego, CA) of the mean and standard deviation (SD) or standard error of mean (SEM) of at least triplicate samples for each biological assay. Student *t* tests were used to calculate statistical significance (GraphPad Prism) and a *P*-value less than 0.05 was considered to be significant.

Results

*Effect of **1** on PDAC cell proliferation and apoptosis*

The synthesis and pharmaceutical properties of compound **1** were reported previously [13-15]. **1** potently and selectively inhibited proliferation of a number of commercially available and patient-derived PDAC cell lines examined (i.e., IC_{50s} of 15, 12, 12, 13, 9.8 and 8.7 nmol/L for LM-P, MIA PaCa-2, HPAC, BxPC-3, AsPC-1, 779E and 1334E cells, respectively, **Table 1**) but was not acutely cytotoxic to cancer cells or normal cells [13]. **1** also potently activated apoptosis (i.e., activation of caspase-3/7 activity) in five of the seven PDAC cells examined (i.e., EC_{50s} of 3.5, 16, 14, 12 and 11 nmol/L in LM-P, MIA PaCa-2, HPAC, BxPC-3 and 1334E cells, respectively, **Table 1**). The EC_{50} values for induction of apoptosis were consistent with the IC_{50s} for inhibition of PDAC cell proliferation (**Table 1**). Stimulation of apoptosis by **1** was apparently dependent on the presence of a full-length p53 protein because apoptosis was not observed for **1** (up to 5000 nmol/L) in AsPC-1 and 779E cells with a p53 frameshift or premature stop mutation (i.e., truncated p53, comparable with p53 knockout mutations) [31].

*Effect of **1** on the activation of DNA damage checkpoint*

Compound **1** (i.e., 40 nmol/L, 4 hours) increased the amount of phospho(Ser428)-Ataxia Telangiectasia and Rad3-related protein kinase (p-ATR) and phospho(Ser1981)-Ataxia-Telangiectasia Mutated kinase (p-ATM) protein in LM-P, MIA PaCa-2, HPAC and BxPC-3 cells (**Figure 1B**) in a dose-dependent manner (i.e., EC_{50s} of 10, 24, 16 nmol/L for p-ATM in MIA PaCa-2, HPAC and BxPC-3 cells, respectively, and EC_{50s} of 9.3, 8.2, 43 nmol/L for p-ATR in LM-P, MIA PaCa-2 and HPAC cells, respectively; Table S2 and Figure S1). EC_{50s} observed were consistent with values of proliferation inhibition and apoptosis induction (Student *t* test; *P*> 0.1; **Table 1**). Data showed **1** activated ATM/ATR phosphorylation to activate DNA damage checkpoint. As reported previously for colorectal cancer cells [13], **1** caused a similar effect in inducing microtubule disruption in PDAC cells (Table S2 and Figure S2A-D), that was more potent than the typical microtubule destabilizer (i.e., colchicine) (Figure S2B, S2C).

*Effect of **1** on p53 and phosphorylated-p53 in whole-cell extracts*

The effect of **1** (i.e., 40 nmol/L, 4 hours) on the activation of total p53, phospho(Ser15)-p53 and phospho(Ser46)-p53 differed for different

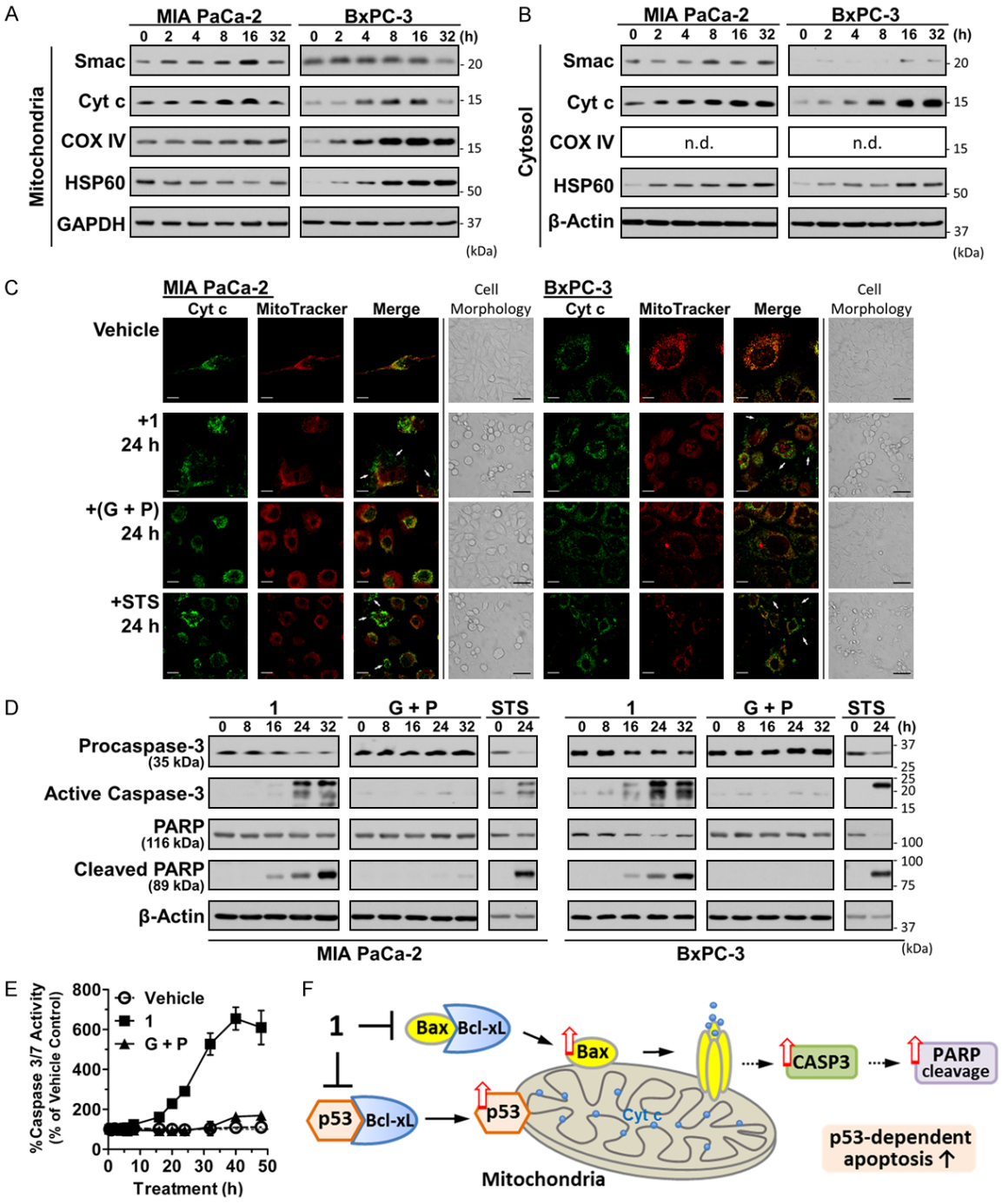

Figure 2. Effect of **1** on time-dependent release of apoptotic markers and activation of caspases. (A, B) Western blot analysis of **1** on Smac, cytochrome c (Cyt c), COX IV, HSP60 as determined from mitochondrial (A) and cytosolic (B) extract of MIA PaCa-2 and BxPC-3 cells. (C) Representative immunofluorescence images of cytochrome c and MitoTracker labeling of mitochondria in MIA PaCa-2 and BxPC-3 cells and corresponding cell morphology images treated with Veh, **1**, Gemcitabine and Paclitaxel (G+P) or Staurosporine (STS) for 24 hours. Scale bar for immunofluorescence images: 10 μm; scale bar for cell morphology images: 50 μm. The arrows show cytochrome c release from mitochondria to cytosol. (D) Western blot analysis of **1** on Procaspase-3, active Caspase-3 (cleaved), PARP (full length) and cleaved PARP as determined from whole-cell extracts of MIA PaCa-2 and BxPC-3 cells compared to Gemcitabine and Paclitaxel (G+P) or Staurosporine (STS). (E) Activation of Caspase-3/7 activity by **1** determined by a Caspase-Glo 3/7 Assay compared to Gemcitabine and Paclitaxel (G+P). Concentrations used: **1**, 50 nmol/L; Gemcitabine, 50 nmol/L; Paclitaxel, 5 nmol/L and Staurosporine, 1 μmol/L. Veh, vehicle control (0.5% DMSO). Treatment time was from 0 to 32 hours. GAPDH used as a mitochondrial internal control and β-Actin was used as an internal control of

cytosolic and whole-cell extracts. Data are mean ± SD (n=3) in (E); n.d., not detected. (F) Proposed working mechanism of **1** in the activation of PDAC cell apoptosis through p53-dependent, mitochondrial-related pathway.

cell types with distinct p53 mutant status (whole-cell extract; **Figure 1C**). In cells with wild-type p53 (i.e., HPAC), **1** increased the amount of phospho(Ser15)-p53, phospho-(Ser46)-p53 and total p53 protein in a dose-dependent manner (i.e., EC_{50s}, 10-100 nmol/L; Table S2 and Figure S1). In cells with missense p53 mutations (i.e., LM-P, MIA PaCa-2, BxPC-3, **Table 1**), **1** modestly increased p53 or phosphorylated p53 protein levels (within 2-fold, 4 hours treatment). In contrast, colchicine (i.e., 8-5000 nmol/L) had no apparent effect on the amount of total p53 in LM-P cells (Figure S3A). These results showed p53 activation by **1** was not simply a matter of an effect on p53 stabilization or on immediate activation of phosphorylation (activated phospho(Ser15)-p53 levels were observed after 16 hours treatment, Figure S4) in PDAC cells with mutant p53.

*Effect of **1** on antagonizing the anti-apoptotic roles of Bcl-xL*

Compound **1** did not cause accumulation of p53 in the nucleus of Mia PaCa-2 or BxPC-3 cells (Figure S5). This result suggested **1** may work through cytoplasmic p53-dependent pathways. Based on immunoprecipitation of Bcl-xL with cytosolic protein extracts of MIA PaCa-2 and BxPC-3 cells, **1** (i.e., 50 nmol/L, 4 hours) was shown to disrupt p53·Bcl-xL and Bax·Bcl-xL complexes in the cytosol to liberate p53 and Bax (**Figure 1D**). Compound **1** antagonized the anti-apoptotic roles of Bcl-xL and then activated mitochondrial-dependent apoptosis signaling.

*Effect of **1** on mitochondrial p53-dependent apoptosis*

Compound **1** (i.e., 50 nmol/L; 2-32 hours) caused translocation and accumulation of p53, phospho(Ser15)-p53 and other pro-apoptotic proteins (i.e., Bax, Bak, Bid, Bad, **Figure 1E-H**) to the mitochondria although there were no detectable changes in the levels of those proteins in total protein extracts (Figure S4). In contrast, colchicine (i.e., 200 nmol/L, 4 hours) had no detectable effect on dissociation of p53·Bcl-xL complex or mitochondrial accumulation of pro-apoptotic markers (Figure S3B, S3C). The pattern differed among different protein markers: p53 and phospho(Ser15)-p53 accumulated in the mitochondrial fraction in a time-dependent fashion (**Figure 1E**, **1F**) after 4 hours treatment in MIA PaCa-2 and BxPC-3 cells. An increase of p53 or phospho(Ser15)-p53 was less apparent in cytosolic fractions (**Figure 1G**, **1H**). Pro-apoptotic markers (i.e., Bax, Bak, Bad and Bid) accumulated (and/or translocated) into the mitochondria from cytosol (i.e., Bax, >2-fold; Bak, >10-fold; Bad, >4-fold; Bid, >3-fold; **Figure 1E-H**) in a time-dependent fashion. This effect was also observed in HPAC cells with wild-type p53 (Figure S6). Anti-apoptotic marker Bcl-xL and Mcl-1 also translocated into the mitochondria (i.e., Bcl-xL, >2-fold; Mcl-1, >5-fold; **Figure 1E**, **1F**) from cytosol (**Figure 1G**, **1H**) in a time-dependent fashion. In view of the anti-apoptotic roles of Bcl-xL and Mcl-1, this apparent translocation effect caused by **1** may be related to a balance in cell death due to impairment of mitochondrial integrity and function [32]. However, accumulation of Bcl-xL and Mcl-1 in the mitochondria ceased at 8-16 hours post-treatment and total protein levels of Bcl-xL and Mcl-1 decreased in both a time-dependent and dose-dependent manner (i.e., IC_{50s} of 11-46 nmol/L for Bcl-xL; Table S2 and Figure S4). These results provided further support for induction of apoptosis by **1**.

*Effect of **1** on cytochrome c release and caspases activation*

Compound **1** (i.e., 50 nmol/L) induced additional apoptotic activators (i.e., Smac, Cytochrome c, HSP60) release into cytosol and the downstream apoptosis (**Figure 2A-E**). The pattern of release varied among different protein markers: *i) Activator of Caspases: Smac, Cytochrome c, COX IV, HSP60.* Cytochrome c (Cyt c) accumulated in both mitochondria and cytosolic fractions in BxPC-3 cells and to a lesser extent in MIA PaCa-2 cells in a time-dependent fashion (**Figure 2A**, **2B**). Mitochondrial accumulation of Cyt c decreased at 16-32 hours, but the

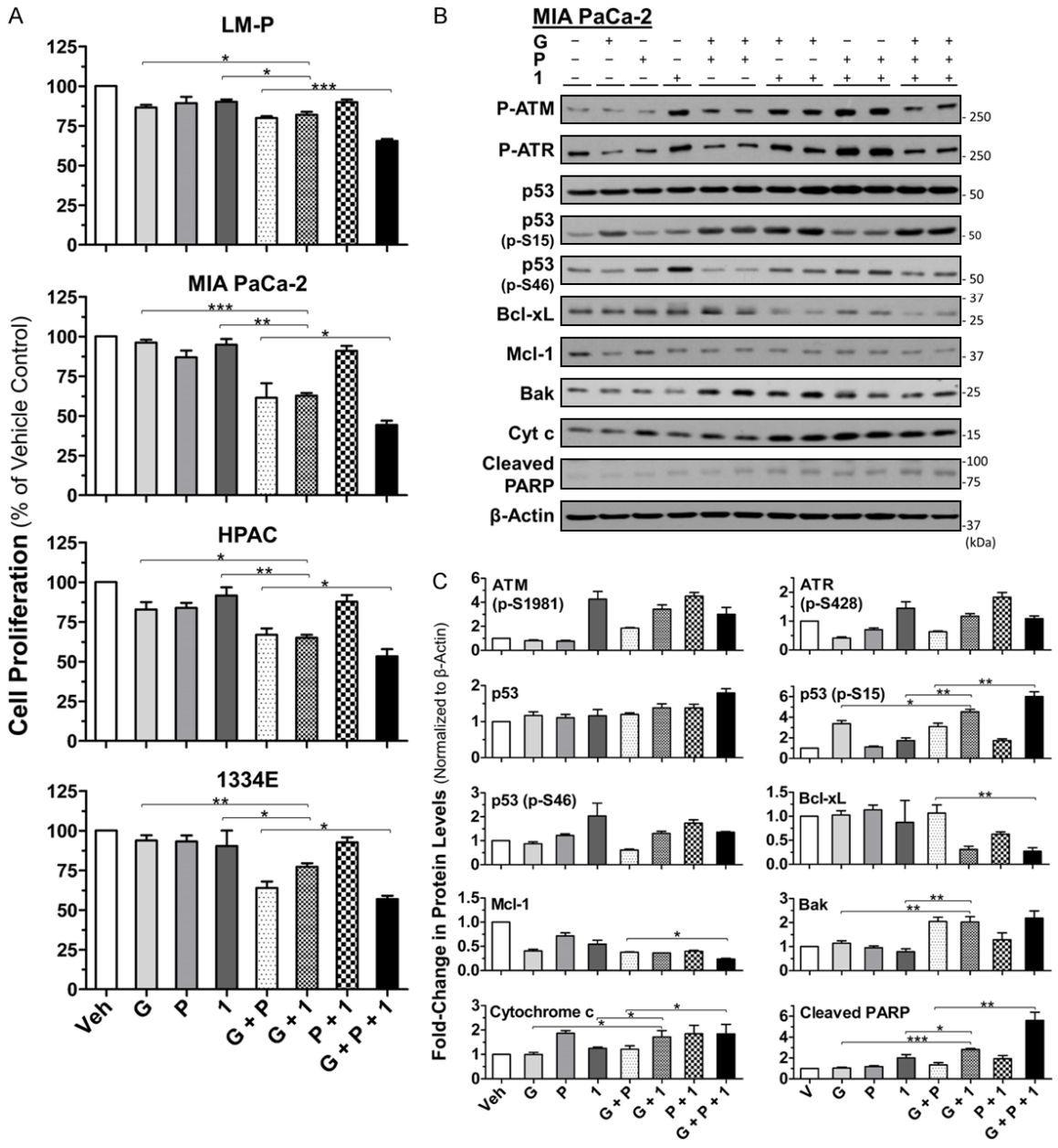

Figure 3. Effect of **1** on PDAC cell proliferation and protein levels of DNA damage and apoptotic markers in the presence of gemcitabine and/or paclitaxel. (A) Inhibition of PDAC cell proliferation by gemcitabine (G, 2-4 nmol/L) and/or paclitaxel (P, 1-2 nmol/L) in the presence of **1** (2-8 nmol/L) is significantly enhanced compared to single agent treatment. The doses used: LM-P (1, 2 nmol/L; P, 1 nmol/L; G, 4 nmol/L); MIA PaCa-2 (1, 2 nmol/L; P, 1 nmol/L; G, 2 nmol/L); HPAC (1, 8 nmol/L; P, 2 nmol/L; G, 4 nmol/L) and 1334E (1, 4 nmol/L; P, 1 nmol/L; G, 2 nmol/L). (B) Western blot and (C) densitometry analysis of the combination of gemcitabine (G, 50 nmol/L) and/or paclitaxel (P, 5 nmol/L) in the presence of **1** (50 nmol/L) on phospho(Ser1981)-ATM, phospho(Ser428)-ATR, p53, phospho(Ser15)-p53, phospho(Ser46)-p53, Bcl-xL, Mcl-1, Bak, cytochrome c or cleaved PARP as determined from whole-cell extracts of MIA PaCa-2 cells. Treatment time was 16 hours. β-Actin was used as an internal control. Data represents the mean ± SD (n=6) of cell proliferation (%) in (A) or mean ± SD (n=3) of protein fold-changes in (C) as determined for compound-treated samples relative to vehicle control. Veh, vehicle control (0.5% DMSO); P, paclitaxel; and G, gemcitabine. *P*-values were estimated by Student *t* tests (**P*<0.05, ***P*<0.01, ****P*<0.001).

onset of cytochrome c release showed it occurred at a later time (>16 hours) than other pro-apoptotic marker accumulation (4-8 hours). COX IV (cytochrome c oxidase) accumulated

Table 2. Effect of compound **1** in the presence of gemcitabine (G) and/or paclitaxel (P) on LM-P, MIA PaCa-2 or HPAC cell proliferation

Treatment[a]	Combination Index (CI)[b]					
	LM-P		MIA PaCa-2		HPAC	
	ED_{75}[c]	ED_{90}[c]	ED_{75}[c]	ED_{90}[c]	ED_{75}[c]	ED_{90}[c]
G+P	0.67	0.67	0.62	0.57	1.12	0.51
G+1	0.73	0.48	0.44	0.26	0.42	0.33
P+1	1.48	2.58	1.10	1.61	2.61	6.56
G+P+1	0.67	0.54	0.56	0.36	0.85	0.44

[a]**1**, compound **1**; G, gemcitabine; P, paclitaxel. [b]Combination Index, (CI) values were calculated based on the Chou-Talalay method [27]; Values of CI<1, =1 and >1 indicate synergism, additive and antagonism, respectively. [c]$ED_{75, 90}$ represent concentrations that cause 75%, 90% of proliferation inhibition, respectively.

and was only detected in mitochondrial protein extracts as a mitochondrial marker. The changes in Cyt c were confirmed by immunofluorescence microscopy (**Figure 2C**). Cytochrome c in vehicle-treated MIA PaCa-2 or BxPC-3 cells co-localized with MitoTracker labeling in the mitochondria. At progressively later stages of apoptosis (24 hours), fragmented mitochondria was observed and most mitochondria had lost its structure as indicated by MitoTracker labeling (shown in MIA PaCa-2 cells, **Figure 2C**). Following complete release, Cyt c was no longer within the mitochondria (i.e., Cyt c was not co-localized with MitoTracker, **Figure 2C**) but became visible in the cytosol. Cyt c release became prominent in **1**-(50 nmol/L) or staurosporine (STS; 1 μmol/L)-treated cells but not in gemcitabine (G; 50 nmol/L) with paclitaxel (P; 5 nmol/L)-treated cells at 24 hours (**Figure 2C**). This provided direct confirmation of Western blot data and also showed that loss of intact mitochondrial structure caused Cyt c release into cytosol. Furthermore, based on subcellular fractionation and immunoblotting results (**Figure 2A**, **2B**), proteins much larger than Cyt c (i.e., Smac, 25 kDa; HSP60, 60 kDa) were also released from mitochondria. Smac and HSP60 followed a similar translocation timeline as Cyt c (**Figure 2A**, **2B**). The increase of those proteins in the total protein extract was not as apparent as observed in subcellular fractionation immunoblots (Figure S4). *ii) Activation of Caspase-3.* Decrease of procaspase-3 (i.e., precursor and inactive form of Caspase-3, 35 kDa) was observed in both MIA PaCa-2 and BxPC-3 cells in the presence of **1** (i.e., 50 nmol/L; **Figure 2D**). The presence of maximum functional caspase-3 (i.e., cleaved forms, 15-23 kDa) was observed at 16-32 hours in MIA PaCa-2 and BxPC-3 cells. This result was similar to that observed in STS (1 μmol/L)-treated cells and also consistent with observations of highly induced Caspase-3/7 (i.e., >6-fold at >24 hours) in the presence of **1** in PDAC cells as determined by Caspase 3/7 activity measurement (**Table 1**; **Figure 2E**). For comparison, "G+P" did not activate caspase-3 protein within 32 hours (**Figure 2D**) and only activated Caspase-3/7 activity ~1.5-fold at >40 hours (**Figure 2E**). *iii) PARP Cleavage.* **1** (i.e., 50 nmol/L) potently induced cleavage of PARP (i.e., 16 hours, **Figure 2D**) in PDAC cells. A time point of 16 hours was also consistent with the release of Cyt c determined by immunofluorescence (**Figure 2C**). The EC_{50s} of **1** for PARP cleavage (i.e., 21 and 29 nmol/L in MIA PaCa-2 and BxPC-3, respectively; Table S2; Figure S7) were similar to IC_{50s} observed in other *in vitro* assays (i.e., IC_{50s} 12-16 nmol/L for both cell proliferation and apoptosis; **Table 1**). In contrast, treatment of MIA PaCa-2 or BxPC-3 cells with "G+P" induced PARP cleavage at much later time (i.e., >32 hours). Compare to other clinical drugs or drug combinations (e.g., G+P), activation of Caspase-3 and PARP cleavage showed that **1** more potently induced PDAC cell apoptosis with greater potency and at an earlier time point (i.e., 16 hours). Treatment of MIA PaCa-2 and BxPC-3 cells with **1** showed similar behavior as apoptosis inducer STS but 20-fold greater concentrations of STS were required (i.e., 1, 50 nmol/L compared to STS, 1 μmol/L). Thus, with regard to apoptosis in MIA PaCa-2 or BxPC-3 cells, the potency of **1** compared very favorably to gemcitabine plus paclitaxel that is one of the most effective treatments for PDAC [7, 8, 33, 34] but acted at an earlier time point.

*Synergistic effect of **1** with gemcitabine and paclitaxel in PDAC cells*

Gemcitabine and paclitaxel have been reported to inhibit the proliferation of PDAC cells with

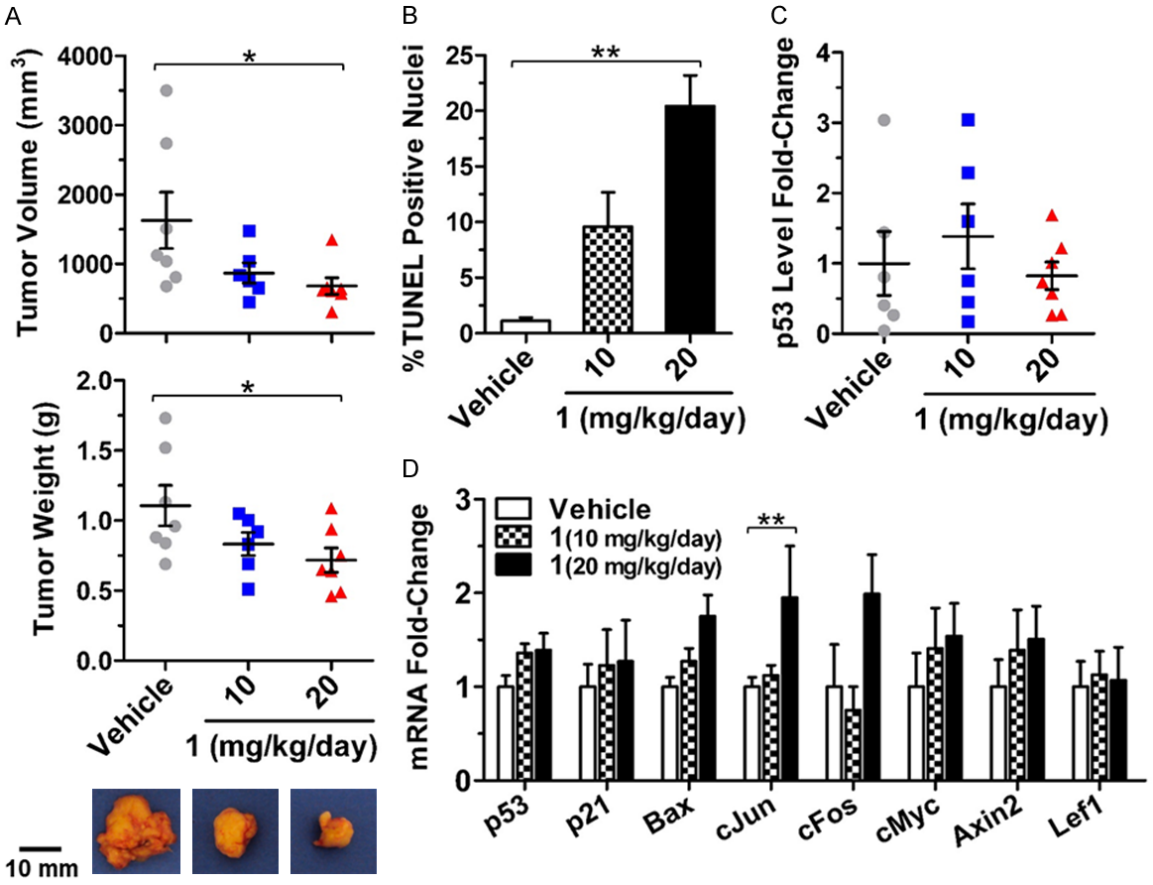

Figure 4. (A) Tumor volume (mm^3) and weight (g) for samples excised from orthotopic mice treated with vehicle or two different doses of **1** (daily, 28 days, i.p.) and representative tumor images. The induction of apoptosis in tumor tissue was evaluated by TUNEL staining: (B) Percentage of TUNEL-positive nuclei (apoptotic index) was calculated. (C) Western blot analysis of total p53 proteins and (D) relative mRNA levels of apoptotic and Wnt target gene expression from tissue extracts of tumors from animals of (A) (day 28). Circle, vehicle (aqueous-DMSO-captisol), n=7; Square, 10 mg/kg/day of **1**, n=6; triangle, 20 mg/kg/day of **1**, n=7 in (A and C); White bar, vehicle; hatched bar, 10 mg/kg/day of **1**; black bar, 20 mg/kg/day of **1** in (B and D). Data are mean ± SEM in (A-C) and mean ± SD in (D). *P*-values were estimated by Student *t* tests (**P*<0.05, ***P*<0.01).

IC_{50s} from 8 nmol/L to 24 μmol/L and 10 nmol/L to 5 μmol/L, respectively [35, 36]. In our hands, the potency of these two anti-cancer drugs in PDAC cells was significant (i.e., IC_{50s} of 5.5-31 nmol/L and 1.3-8.6 nmol/L, respectively; Table S3). However, in the presence of **1** (i.e., 2-8 nmol/L), combination treatment inhibited cell proliferation significantly greater (i.e., *P*<0.05) than gemcitabine alone (i.e., 2-8 nmol/L) or gemcitabine with paclitaxel (i.e., 1-2 nmol/L) (**Figure 3A**). This effect was also observed in patient-derived human primary PDAC cells (i.e., 1334E; **Figure 3A**). Based on a Chou-Talalay synergism analysis (**Table 2**) [27], **1** synergistically enhanced the inhibitory effect on proliferation of LM-P, MIA PaCa-2 and HPAC cells with gemcitabine alone or gemcitabine plus paclitaxel, and showed a low value "combination index" (CI<1). There was antagonism (i.e., CI>1; **Table 2**) between **1** and paclitaxel because they work at least in part at similar sites (i.e., microtubule) and have opposite function [13].

Enhancement of inhibition of cell proliferation was p53-dependent because enhancement was not observed in AsPC-1 and 779E cells (i.e., $^{-/-}$p53 cells, Figure S8A-C). As shown in **Figure 3B**, **3C**, ATM/ATR auto-phosphorylation in MIA PaCa-2 cells was only observed in **1**-treated cells, but did not enhance the effect in combination-treatment. Neither total p53 nor phospho(Ser46)-p53 was affected by com-

bination-treatment (**Figure 3B**, **3C**). Synergism was associated with increase in phospho-(Ser15)-p53 (activated by **1** in combination with gemcitabine but not paclitaxel). Moreover, inhibition of anti-apoptotic markers (i.e., Bcl-xL, Mcl-1) and activation of apoptotic markers (i.e., Bak, cytochrome c, PARP cleavage) was enhanced by **1** in combination with gemcitabine (but not paclitaxel). Maximal effect was observed for **1** in the presence of both gemcitabine and paclitaxel. In contrast, no apparent synergistic effect (i.e., BxPC-3) or enhancement of phospho(Ser15)-p53 was observed in cells treated with **1** in combination with gemcitabine (Figure S9A, S9B).

*Effect of **1** on tumor growth in an orthotopic model of invasive PDAC*

Previous pharmacokinetics and dynamics studies showed compound **1** possessed sufficient chemical and metabolic stability and bioavailability to study its efficacy in vivo [13]. The efficacy of **1** was examined in an orthotopic PDAC animal model [25]. Compared to vehicle-treated mice, **1** (10 or 20 mg/kg/day; i.p.; 28 days) decreased LM-P tumor growth volume and weight (**Figures 4A** and S10). At the end of the study, excised tumor volumes and weights of **1**-treated mice (20 mg/kg/day, n=7) were significantly lower (i.e., $P<0.05$; 65% and 41%, respectively; **Figure 4A**) than those of vehicle-treated mice (aqueous-DMSO-Captisol, n=7). **1** significantly decreased PDAC growth in vivo. Compared to vehicle-treated mice (n=3), clinical chemistry serum values of **1**-treated mice (20 mg/kg/day, n=3) were similar (Table S4) and were also consistent with normal reported values [37]. This showed that treatment with **1** (20 mg/kg/day; i.p.; 28 days) was not toxic to liver, kidney or blood. The treatment of **1** had little difference in the body weight compared with the control group. (Figure S11). At the end of the study, immunohistochemistry and H&E did not show differences in tissue morphology among the three groups (Figure S12A). Apoptosis marker TUNEL staining showed a significant difference between vehicle-treated and **1**-treated groups (Figure S12B). Compared to vehicle-treated animals, treatment with **1** caused a significantly greater (i.e., $P<0.01$) %TUNEL-positive apoptotic cells from tumors of animals (i.e., 8- and 18-fold increase for 10 and 20 mg/kg/day, respectively; **Figure 4B**).

*Effect of **1** on in vitro and in vivo apoptotic and Wnt target gene expression*

Compared to vehicle-treated animals, total p53 levels in tumors from either 10 mg/kg/day or 20 mg/kg/day **1**-treated animals were not statistically significantly different (**Figures 4C** and S12B). This was consistent with immunoblot analysis of the effect of **1** on p53 in LM-P cells (**Figure 1C**). In addition, compared to vehicle-treated mice, neither *p53* nor *p53* target genes (i.e., *p21*, *Bax*) mRNA were up-regulated in tumor samples from **1**-treated animals (**Figure 4D**). This further showed **1** was working through a mechanism that did not simply affect either *p53* target gene expression or p53 protein stability (especialy in mutant p53 cells). In contrast, tumor tissue samples from **1**-treated animals (20 mg/kg/day) resulted in a 2-fold increase in mRNA levels for pro-apoptotic genes, *cJun* and *cFos* but canonical Wnt target genes, *cMyc* and *Lef1* were not statistically significantly different (**Figure 4D**). These data were consistent with in vitro gene expression in LM-P cells treated with **1** (or colchicine as a control, Figure S3D). For **1**, down-regulation of Wnt target gene expression was less apparent (i.e., within a 2-fold difference) in MIA PaCa-2 cells with mutant p53 status compared to HPAC cells with wild-type p53 status (Figure S13). This effect was also less than that observed previously in other cancer cells (i.e., colon cancer) [13]. The data showed inhibition of Wnt signaling by **1** was not a prominent pathway in PDAC cells, especially those cells with mutant p53 status.

Discussion

Compound **1** showed significant potency in inhibition of cell proliferation and activation of cell apoptosis in PDAC cell models (i.e., LM-P, MIA PaCa-2, etc.). **1** activated upstream DNA-damage via ATR/ATM-kinase activation and further activated apoptosis in mitochondrial p53-dependent pathways. For example, **1** activated cytosolic p53, inhibited binding of cytosolic p53/Bax to anti-apoptotic Bcl-xL, caused

activation of pro-apoptotic p53/Bax and induced mitochondrial cytochrome c release to trigger cell apoptosis (**Figure 2F**).

Mutations of tumor suppressor p53 are among the most common genetic changes in cancer (e.g., ~75% in PDAC) [38]. Mutations of p53 in tumor cells can cause loss of wild-type p53 and gain of novel oncogenic functions (i.e., regulation of DNA damage-induced apoptotic response), leading to metastasis of cancer cells [38, 39] and poor clinical response to cancer chemotherapies [40]. PDAC cell model work reported herein (i.e., LM-P, MIA PaCa-2, etc., **Table 1**) utilized cells with different p53 mutant status. The resistance to other chemotherapy (i.e., gemcitabine, 5-fluorouracil, etc.) normally observed in cancer cells [3-6] with mutant p53 was not observed in PDAC cells treated with **1**. Compared to wild-type p53 cells (i.e., HPAC), cell apoptosis of mutant p53 cancer cells (i.e., LM-P, MIA PaCa-2, etc.) was induced by **1** but without significant up-regulation (<2-fold difference) of p53 or phosphorylation of p53 (**Figure 1C**). However, the lack of stimulation of cell apoptosis by **1** in p53-deficient cell lines (i.e., AsPC-1, 779E; frameshift mutations of *p53*) shows that p53 still plays a significant role in the mechanism of action of **1** to induce cell apoptosis. A mitochondrial p53-dependent apoptosis pathway was proposed to explain cell apoptosis induced by **1** in mutant p53 cells (**Figure 2F**).

In cancer cells, survival factors (i.e., Bcl-2, Bcl-xL and Mcl-1) interact with and antagonize pro-apoptotic Bcl-2 family members (i.e., Bax, Bak, etc.) and p53, block mitochondrial outer-membrane permeabilization (MOMP) and inhibits apoptosis. **1** disrupts these interactions that release p53/Bax to activate translocation of pro-apoptotic Bcl-2 family proteins from the cytosol to the mitochondria. Therefore, activation of apoptotic systems by treatment of **1** in PDAC cells involves loss of mitochondrial membrane integrity and opening of permeability transition pores (i.e., Bak/Bax forms oligomers on the mitochondrial membrane; required for MOMP). As a result, this further induces cytochrome c, Smac and HSP60 release into cytosol that neutralizes inhibition of apoptosis (caspases) and causes incipient apoptotic signaling (i.e., PARP cleavage) [20, 32, 41]. Such a working model differentiates **1** from other microtubule destabilizers (e.g., colchicine, Figure S3B, S3C) because colchicine has no reported effects on apoptosis. This also differentiates **1** from other p53-targeted inhibitors in tumor suppression. P53-dependent cell death checkpoint inhibitors (e.g., Nutlin-3a and Pfithrins) either induce apoptosis of tumor cells or protect normal cells from radio- or chemo-sensitivity [42, 43]. Pfithrins (PFT-α, -μ) reversibly block p53-dependent apoptosis of normal cells via transactivation-dependent or -independent mechanisms [44, 45] but do not induce apoptosis in mutant p53-bearing PCs. Compound **1** was able to activate the p53 mediated transcriptional-independent mitochondrial-apoptotic pathways in both wild-type p53 (i.e., HPAC) and mutant p53 (i.e., MIA PaCa-2, BxPC-3) PDAC cells.

There was no apparent relationship observed between p53 mutation status and potency of **1** to inhibit cell proliferation in PDAC cells. For example, AsPC-1 cells (135Δ1bp frameshift mutation of *p53*, [31]) responded to **1** with a similar IC_{50} value as that observed in WT *p53* PDAC cells (**Table 1**). However, there was no significant enhancement of inhibition of AsPC-1 cell proliferation with **1** in the presence of chemotoxins (Figure S8B). Similar results were observed in another frameshift mutant *p53* cell line (i.e., 779E; Figure S8C). This suggests p53 activation contributes to the mechanism of action of **1** in the presence of chemotoxins. There was no apparent relationship between p53 mutation status and synergistic effect of chemotoxins in the presence of **1**. The greatest synergistic effect of **1** in the presence of gemcitabine (or gemcitabine with paclitaxel) was observed in LM-P, MIA PaCa-2 and HPAC cells with different p53 mutant status (i.e., Arg172His, Arg248Trp, wild-type p53, respectively; **Table 1**). Therefore, synergistic inhibition of PDAC cell growth in the presence of **1** and chemotoxins likely may be affected by more complex factors other than simple p53 mutation status. Phospho(Ser15)-p53 may be a possible factor that controls the different synergistic effect of **1** observed in different PDAC cells (**Figures 3B**, **3C**, S9A and S9B). Other factors may contribute to lower synergy for **1** in the

presence of chemotherapeutics. For example, BxPC-3 cells (Tyr220Cys p53) also possess wild-type K-Ras [46] and this may have an effect (Figure S8A).

Compound **1** was found to disrupt microtubule structure in PDAC cells in a similar manner to that observed in other cancer types (i.e., potent thermodynamic binding properties with tubulin) [13]. This may contribute to the considerable efficacy and lack of toxicity observed for **1** [13]. qPCR analysis of in vitro (Figure S3D) and in vivo samples (**Figure 4D**) showed that c-Jun N-terminal kinase (JNK) signaling (i.e., *cJun*, *cFos*) was activated by **1** similarly as other microtubule damaging agents (i.e., colchicine, Figure S3D) [47]. However, mitochondrial p53-dependent apoptosis activation was only observed for treatment with **1** and not for colchicine (Figure S2A-C).

An induced Wnt pathway is often observed in different types of cancer [10]. As previously reported [13], **1** exerts its effects on Wnt signaling inhibition via HIPK2 and TCF proteins (TCF4, LEF1, TCF3) by decreasing active TCF proteins available for stimulation of transcription of Wnt target genes. This was linked to p53 activation via phospho(Ser46)-p53 [13]. However, in PDAC cells with mutant p53 status, no detectable effect of **1** on Wnt target gene expression (i.e., *cMyc*, *Lef1*) was observed. Likewise, no immediate activation (i.e., treatment time, 2-4 hours) of phospho(Ser46)-p53 or phosphorylated-HIPK2 and TCF3 by **1** was observed in PDAC cells examined (**Figures 1C** and S14). It may be that mutation status of p53 in PDAC cells contributes to some feedback-loop effect on the function of HIPK2 that may indirectly affect the Wnt pathway. Inhibition of Wnt-dependent transcription by **1** (through HIPK2 and TCF pathways) is likely not a major pathway in the mechanism of action of **1** in PDAC cells with mutated p53.

Gemcitabine is a standard systemic chemotherapeutic agent for PDAC tumors, but outcome after treatment with gemcitabine alone and in the presence of other drugs remain disappointing [3, 4]. Mice inoculated with PDAC and treated with gemcitabine (100 mg/kg/4 days; 9 days; i.p.) plus nab-paclitaxel (120 mg/kg/4 days; 9 days; i.v.) affords an estimated 50% inhibition of tumor growth (compared to vehicle-treated mice) [34]. This is a somewhat lower level of tumor growth inhibition compared to treatment of 20 mg/kg/day of **1** (i.e., 65% inhibition, **Figure 4A**). Thus, **1** may be equally or more efficacious to the most commonly used clinical combination treatment in an animal model of PDAC.

In summary, compound **1** is a non-toxic, highly efficacious treatment of PDAC that selectively destabilizes microtubule polymerization and results in activation of DNA damage checkpoint- and mitochondrial p53-dependent apoptosis. **1** showed considerable synergism with commonly used combination therapy in the treatment of PDAC. **1** also inhibited tumor growth in an orthotopic model of invasive PDAC cells (LM-P). Because of its novel mechanism of action, compound **1** has broad utility to treat pancreatic cancer.

Acknowledgements

We thank Charitha Madiraju, Ph.D., for helpful discussions. This work was supported by Small Business Technology Transfer Program Grant from the Department of Health (R41CA176931; J.R. Cashman), and Discovery Stage Research Projects: Inception Award from California Institute for Regenerative Medicine (CIRM) (DISC1-10583; J.R. Cashman), and Human Services and Research Project Grant from NIH (RO1CA155620, A.M. Lowy) as well as by funds from the Human BioMolecular Research Institute.

Disclosure of conflict of interest

None.

Address correspondence to: Dr. Jiongjia Cheng, Human BioMolecular Research Institute, 5310 Eastgate Mall, San Diego, CA 92121, USA. Tel: 858-458-9305; Fax: 858-458-9311; E-mail: jcheng@hbri.org

References

[1] Siegel RL, Miller KD and Jemal A. Cancer statistics, 2018. CA Cancer J Clin 2018; 68: 7-30.

[2] Rahib L, Smith BD, Aizenberg R, Rosenzweig AB, Fleshman JM and Matrisian LM. Projecting

cancer incidence and deaths to 2030: the unexpected burden of thyroid, liver, and pancreas cancers in the United States. Cancer Res 2014; 74: 2913-2921.

[3] Burris H and Storniolo AM. Assessing clinical benefit in the treatment of pancreas cancer: gemcitabine compared to 5-fluorouracil. Eur J Cancer 1997; 33 Suppl 1: S18-22.

[4] Burris HA 3rd, Moore MJ, Andersen J, Green MR, Rothenberg ML, Modiano MR, Cripps MC, Portenoy RK, Storniolo AM, Tarassoff P, Nelson R, Dorr FA, Stephens CD and Von Hoff DD. Improvements in survival and clinical benefit with gemcitabine as first-line therapy for patients with advanced pancreas cancer: a randomized trial. J Clin Oncol 1997; 15: 2403-2413.

[5] Conroy T, Desseigne F, Ychou M, Bouché O, Guimbaud R, Bécouarn Y, Adenis A, Raoul JL, Gourgou-Bourgade S, de la Fouchardière C, Bennouna J, Bachet JB, Khemissa-Akouz F, Péré-Vergé D, Delbaldo C, Assenat E, Chauffert B, Michel P, Montoto-Grillot C, Ducreux M; Groupe Tumeurs Digestives of Unicancer; PRODIGE Intergroup. FOLFIRINOX versus gemcitabine for metastatic pancreatic cancer. N Engl J Med 2011; 364: 1817-1825.

[6] Moore MJ, Goldstein D, Hamm J, Figer A, Hecht JR, Gallinger S, Au HJ, Murawa P, Walde D, Wolff RA, Campos D, Lim R, Ding K, Clark G, Voskoglou-Nomikos T, Ptasynski M, Parulekar W; National Cancer Institute of Canada Clinical Trials Group. Erlotinib plus gemcitabine compared with gemcitabine alone in patients with advanced pancreatic cancer: a phase III trial of the national cancer institute of canada clinical trials group. J Clin Oncol 2007; 25: 1960-1966.

[7] Goldstein D, El-Maraghi RH, Hammel P, Heinemann V, Kunzmann V, Sastre J, Scheithauer W, Siena S, Tabernero J, Teixeira L, Tortora G, Van Laethem JL, Young R, Penenberg DN, Lu B, Romano A and Von Hoff DD. nab-Paclitaxel plus gemcitabine for metastatic pancreatic cancer: long-term survival from a phase III trial. J Natl Cancer Inst 2015; 107.

[8] Von Hoff DD, Ervin T, Arena FP, Chiorean EG, Infante J, Moore M, Seay T, Tjulandin SA, Ma WW, Saleh MN, Harris M, Reni M, Dowden S, Laheru D, Bahary N, Ramanathan RK, Tabernero J, Hidalgo M, Goldstein D, Van Cutsem E, Wei X, Iglesias J and Renschler MF. Increased survival in pancreatic cancer with nab-paclitaxel plus gemcitabine. N Engl J Med 2013; 369: 1691-1703.

[9] Ansari D, Tingstedt B, Andersson B, Holmquist F, Sturesson C, Williamsson C, Sasor A, Borg D, Bauden M and Andersson R. Pancreatic cancer: yesterday, today and tomorrow. Future Oncol 2016; 12: 1929-1946.

[10] Pasca di Magliano M, Biankin AV, Heiser PW, Cano DA, Gutierrez PJ, Deramaudt T, Segara D, Dawson AC, Kench JG, Henshall SM, Sutherland RL, Dlugosz A, Rustgi AK and Hebrok M. Common activation of canonical Wnt signaling in pancreatic adenocarcinoma. PLoS One 2007; 2: e1155.

[11] Moore PS, Beghelli S, Zamboni G and Scarpa A. Genetic abnormalities in pancreatic cancer. Mol Cancer 2003; 2: 7.

[12] Rozenblum E, Schutte M, Goggins M, Hahn SA, Panzer S, Zahurak M, Goodman SN, Sohn TA, Hruban RH, Yeo CJ and Kern SE. Tumor-suppressive pathways in pancreatic carcinoma. Cancer Res 1997; 57: 1731-1734.

[13] Cheng J, Dwyer M, Okolotowicz KJ, Mercola M and Cashman JR. A novel inhibitor targets both wnt signaling and ATM/p53 in colorectal cancer. Cancer Res 2018; 78: 5072-5083.

[14] Okolotowicz KJ, Dwyer M, Ryan D, Cheng J, Cashman EA, Moore S, Mercola M and Cashman JR. Novel tertiary sulfonamides as potent anti-cancer agents. Bioorg Med Chem 2018; 26: 4441-4451.

[15] Cashman JR, Mercola M, Schade D and Tsuda M. Compounds for inhibition of cancer cell proliferation. Google Patents 2013; US 13/748,770.

[16] Guchelaar HJ, ten Napel CH, de Vries EG and Mulder NH. Clinical, toxicological and pharmaceutical aspects of the antineoplastic drug taxol: a review. Clin Oncol (R Coll Radiol) 1994; 6: 40-48.

[17] Goggins M, Kern SE, Offerhaus JA and Hruban RH. Progress in cancer genetics: lessons from pancreatic cancer. Ann Oncol 1999; 10 Suppl 4: 4-8.

[18] Chipuk JE and Green DR. Cytoplasmic p53: bax and forward. Cell Cycle 2004; 3: 429-431.

[19] Moll UM, Wolff S, Speidel D and Deppert W. Transcription-independent pro-apoptotic functions of p53. Curr Opin Cell Biol 2005; 17: 631-636.

[20] Vaseva AV and Moll UM. The mitochondrial p53 pathway. Biochim Biophys Acta 2009; 1787: 414-420.

[21] Suen DF, Norris KL and Youle RJ. Mitochondrial dynamics and apoptosis. Genes Dev 2008; 22: 1577-1590.

[22] Chipuk JE, Bouchier-Hayes L and Green DR. Mitochondrial outer membrane permeabilization during apoptosis: the innocent bystander scenario. Cell Death Differ 2006; 13: 1396-1402.

[23] Fiorini C, Cordani M, Padroni C, Blandino G, Di Agostino S and Donadelli M. Mutant p53 stimulates chemoresistance of pancreatic adenocarcinoma cells to gemcitabine. Biochim Biophys Acta 2015; 1853: 89-100.

[24] Hingorani SR, Wang L, Multani AS, Combs C, Deramaudt TB, Hruban RH, Rustgi AK, Chang S and Tuveson DA. Trp53R172H and KrasG12D cooperate to promote chromosomal instability and widely metastatic pancreatic ductal adenocarcinoma in mice. Cancer Cell 2005; 7: 469-483.

[25] Tseng WW, Winer D, Kenkel JA, Choi O, Shain AH, Pollack JR, French R, Lowy AM and Engleman EG. Development of an orthotopic model of invasive pancreatic cancer in an immunocompetent murine host. Clin Cancer Res 2010; 16: 3684-3695.

[26] Fujimura K, Wright T, Strnadel J, Kaushal S, Metildi C, Lowy AM, Bouvet M, Kelber JA and Klemke RL. A hypusine-eIF5A-PEAK1 switch regulates the pathogenesis of pancreatic cancer. Cancer Res 2014; 74: 6671-6681.

[27] Chou TC. Drug combination studies and their synergy quantification using the Chou-Talalay method. Cancer Res 2010; 70: 440-446.

[28] Wieckowski MR, Giorgi C, Lebiedzinska M, Duszynski J and Pinton P. Isolation of mitochondria-associated membranes and mitochondria from animal tissues and cells. Nat Protoc 2009; 4: 1582-1590.

[29] Golde WT, Gollobin P and Rodriguez LL. A rapid, simple, and humane method for submandibular bleeding of mice using a lancet. Lab Anim (NY) 2005; 34: 39-43.

[30] Livak KJ and Schmittgen TD. Analysis of relative gene expression data using real-time quantitative PCR and the 2-ΔΔCT method. Methods 2001; 25: 402-408.

[31] Redston MS, Caldas C, Seymour AB, Hruban RH, da Costa L, Yeo CJ and Kern SE. p53 mutations in pancreatic carcinoma and evidence of common involvement of homocopolymer tracts in DNA microdeletions. Cancer Res 1994; 54: 3025-3033.

[32] Chandra D, Liu JW and Tang DG. Early mitochondrial activation and cytochrome c up-regulation during apoptosis. J Biol Chem 2002; 277: 50842-50854.

[33] Borazanci E and Von Hoff DD. Nab-paclitaxel and gemcitabine for the treatment of patients with metastatic pancreatic cancer. Expert Rev Gastroenterol Hepatol 2014; 8: 739-747.

[34] Frese KK, Neesse A, Cook N, Bapiro TE, Lolkema MP, Jodrell DI and Tuveson DA. nab-Paclitaxel potentiates gemcitabine activity by reducing cytidine deaminase levels in a mouse model of pancreatic cancer. Cancer Discov 2012; 2: 260-269.

[35] Awasthi N, Zhang C, Schwarz AM, Hinz S, Wang C, Williams NS, Schwarz MA and Schwarz RE. Comparative benefits of Nab-paclitaxel over gemcitabine or polysorbate-based docetaxel in experimental pancreatic cancer. Carcinogenesis 2013; 34: 2361-2369.

[36] Rathos MJ, Joshi K, Khanwalkar H, Manohar SM and Joshi KS. Molecular evidence for increased antitumor activity of gemcitabine in combination with a cyclin-dependent kinase inhibitor, P276-00 in pancreatic cancers. J Transl Med 2012; 10: 161.

[37] Lillie LE, Temple NJ and Florence LZ. Reference values for young normal Sprague-Dawley rats: weight gain, hematology and clinical chemistry. Hum Exp Toxicol 1996; 15: 612-616.

[38] Deer EL, Gonzalez-Hernandez J, Coursen JD, Shea JE, Ngatia J, Scaife CL, Firpo MA and Mulvihill SJ. Phenotype and genotype of pancreatic cancer cell lines. Pancreas 2010; 39: 425-435.

[39] Freed-Pastor WA and Prives C. Mutant p53: one name, many proteins. Genes Dev 2012; 26: 1268-1286.

[40] Xu J, Wang J, Hu Y, Qian J, Xu B, Chen H, Zou W and Fang JY. Unequal prognostic potentials of p53 gain-of-function mutations in human cancers associate with drug-metabolizing activity. Cell Death Dis 2014; 5: e1108.

[41] Galluzzi L, Morselli E, Kepp O, Tajeddine N and Kroemer G. Targeting p53 to mitochondria for cancer therapy. Cell Cycle 2008; 7: 1949-1955.

[42] Sriraman A, Radovanovic M, Wienken M, Najafova Z, Li Y and Dobbelstein M. Cooperation of Nutlin-3a and a Wip1 inhibitor to induce p53 activity. Oncotarget 2016; 7: 31623-31638.

[43] Vassilev LT, Vu BT, Graves B, Carvajal D, Podlaski F, Filipovic Z, Kong N, Kammlott U, Lukacs C, Klein C, Fotouhi N and Liu EA. In vivo activation of the p53 pathway by small-molecule antagonists of MDM2. Science 2004; 303: 844-848.

[44] Komarov PG, Komarova EA, Kondratov RV, Christov-Tselkov K, Coon JS, Chernov MV and Gudkov AV. A chemical inhibitor of p53 that protects mice from the side effects of cancer therapy. Science 1999; 285: 1733-1737.

[45] Strom E, Sathe S, Komarov PG, Chernova OB, Pavlovska I, Shyshynova I, Bosykh DA, Burdelya LG, Macklis RM, Skaliter R, Komarova EA and Gudkov AV. Small-molecule inhibitor of p53 binding to mitochondria protects mice from gamma radiation. Nat Chem Biol 2006; 2: 474-479.

[46] Berrozpe G, Schaeffer J, Peinado MA, Real FX and Perucho M. Comparative analysis of mutations in the p53 and K-ras genes in pancreatic cancer. Int J Cancer 1994; 58: 185-191.

[47] Weston CR and Davis RJ. The JNK signal transduction pathway. Curr Opin Genet Dev 2002; 12: 14-21.
[48] Kalthoff H, Schmiegel W, Roeder C, Kasche D, Schmidt A, Lauer G, Thiele HG, Honold G, Pantel K, Riethmüller G, et al. p53 and K-RAS alterations in pancreatic epithelial cell lesions. Oncogene 1993; 8: 289-298.

Supplementary data and methods

Supplementary materials and methods

Chemicals and reagents

The following materials (were purchased from): phosphate buffered solution (PBS), Dulbecco's phosphate buffered solution (DPBS), trypsin-EDTA, DMEM (Corning Inc., Corning, NY); Fetal bovine serum (Atlanta Biologicals, Flowery Branch, GA); SYBR Green I nucleic acid stain in DMSO (Lonza, Allendale, NJ); protease inhibitors (Roche, Indianapolis, IN); Pierce BCA protein assay kit and ECL reagent (Thermo Scientific, Rockford, IL); 30% acrylamide/bis solution, iScript cDNA synthesis kit and iQ SYBR Green supermix (Bio-Rad, Hercules, CA); NuPAGE® Novex 3-8% tris-acetate protein gels, 10 × NuPAGE® tris-acetate SDS running buffer, HiMark™ pre-stained standard and Trizol (Life Technologies, Carlsbad, CA); colchicine (Chem-Impex, Wood Dale, IL); paclitaxel (LC Laboratories, Woburn, MA); gemcitabine (Combi-Blocks, San Diego, CA); Captisol® (Ligand Pharmaceuticals, La Jolla, CA); Triton-X-100, bovine serum albumin fraction V (BSA), EDTA, sodium chloride, nonylphenoxypolyethoxylethanol (NP-40), 3α,12α-dihydroxy-5β-cholanic acid sodium salt (sodium deoxycholate), polyethylene glycol sorbitanmonolaurate (Tween-20), dodecyl sulfate sodium salt (SDS), bicine and bis-tris (Sigma-Aldrich, St. Louis, MO); and other chemicals, reagents, solvents and devices (VWR, San Diego, CA). RIPA buffer: 25 mM Tris-HCl, pH 7.6, 150 mM NaCl, 1% NP-40, 1% sodium doxycholate, 0.1% SDS in the presence of 1 × protease inhibitors.

Instrumentation

Fluorescence was determined using a Tecan SPECTRAFluor Plus plate reader (Tecan, San Jose, CA) and luminescence was recorded on a Wallac Victor plate reader (PerkinElmer, Waltham, MA). RT-PCR was conducted with a Bio-Rad iQ5 thermocycler (Bio-Rad).

Antibodies

The following antibodies were used: anti-p53 (Cell Signaling #9282; Bio-Rad, #MCA1701), anti-phospho-Ser15-p53 (Cell Signaling #9284), anti-phospho-Ser46-p53 (Abcam #ab76242), anti-phospho-Ser1981-ATM (Cell Signaling #5883), anti-ATM (Cell Signaling #2873), anti-phospho-Ser428-ATR (Cell Signaling #2853), anti-ATR (Cell Signaling #2790), anti-Bcl-xL (Cell Signaling #2764; Santa Cruz #sc-8392), anti-Bax (Cell Signaling #5883), anti-Mcl-1 (Santa Cruz #sc-74436), anti-Bak (Santa Cruz #sc-517390), anti-Bad (Santa Cruz #sc-8044), anti-Bid (Santa Cruz #sc-373939), anti-Smac (Santa Cruz #sc-393118), anti-Cytochrome c (Santa Cruz #13156), anti-HSP60 (Santa Cruz #sc-13115), anti-COX IV (Cell Signaling #4850), anti-PARP (Cell Signaling #9532), anti-Caspase-3 (Santa Cruz #sc-7272), anti-Caspase-3 p11 (Santa Cruz #sc-271759), anti-Caspase-3 p17 (Santa Cruz #sc-373730), anti-HIPK2 (Abcam #ab75937), Anti-phospho-Tyr361-HIPH2 (Thermo Scientific #PA5-13045), anti-Lamin A/C (Cell Signaling #2032), anti-β-Actin (Cell Signaling #3700), anti-Gapdh (Santa Cruz #sc-47724), anti-β-tubulin (Sigma #T8328), anti-acetylated-tubulin (Sigma #T7451), anti-tyrosinated-tubulin (Sigma #T9028), goat-anti-mouse-IgG-Alexa488nm (Thermo Fisher Scientific #A11017).

Measurement of soluble and polymerized tubulin in LM-P cells

After treatment with vehicle or 1 (1.6-5000 nM), LM-P cells were lysed in 0.1 M 2-(4-morpholinyl)ethanesulfonic acid (MES) pH 6.8, containing 0.1% Triton X-100, 1 mM $MgSO_4$, 2 mM EGTA, and 4 M glycerol. The supernatant (soluble tubulin fraction) and pellet (polymerized tubulin fraction) were separated by centrifugation at 14,000 × g (10 min) and then resolved by SDS-PAGE followed by Western blotting.

Table S1. Sequences of primers[a] used for SYBR Green Real-Time PCR

Gene	Forward	Reverse
hp53	5'-ACAAGGTTGATGTGACCTGGA-3'	5'-TGTAGACTCGTGAATTTCGCC-3'
hcJun	5'-TCCAAGTGCCGAAAAAGGAAG-3'	5'-CGAGTTCTGAGCTTTCAAGGT-3'
hBax	5'-CCCGAGAGGTCTTTTTCCGAG-3'	5'-CCAGCCCATGATGGTTCTGAT-3'
hcMyc	5'-TCCTTGCAGCTGCTTAGACGC-3'	5'-TGCACCGAGTCGTAGTCGAGG-3'
hAxin2	5'-CTCCTTGGAGGCAAGAGC-3'	5'-GGCCACGCAGCACCGCTG-3'
hCCND1	5'-CGCAAACACGCGCAGACCTTC-3'	5'-TTCAGGCCTTGCACTGCGGCC-3'
hGapdh	5'-CATGTTCCAATATGATTCCACC-3'	5'-CTCCACGACGTACTCAGCG-3'
mp53	5'-AAAGAGAGCGCTGCCCACCT-3'	5'-CTCCCGGAACATCTCGAAGC-3'
mp21	5'-TCAGAGTCTAGGGGAATTGGA-3'	5'-AATCACGGCGCAACTGCT-3'
mBax	5'-TAGCAAACTGGTGCTCAAGG-3'	5'-TCTTGGATCCAGACAAGCAG-3'
mcJun	5'-CCTTCTACGACGATGCCCTC-3'	5'-GGTTCAAGGTCATGCTCTGTTT-3'
mcFos	5'-AAACCGCATGGAGTGTGTTGTTCC-3'	5'-TCAGACCACCTCGACAATGCATGA-3'
mcMyc	5'-AGCTGTTTGAAGGCTGGATT-3'	5'-AATAGGGCTGTACGGAGTCG-3'
mLef1	5'-TCACTGTCAGGCGACACTTC-3'	5'-TGAGGCTTCACGTGCATTAG-3'
mActb	5'-AGTGTGACGTTGACATCCGT-3'	5'-TGCTAGGAGCCAGAGCAGTA-3'
36B4	5'-GTGTTCGACAATGGCAGCAT-3'	5'-GACACCCTCCAGGAAGCGA-3'

[a]Primers were designed to have an efficiency of 95% and purchased from ValueGene (San Diego, CA) or Eton Bioscience (San Diego, CA). qPCR incubations were run using a Bio-Rad iQ5 thermocycler under the following conditions: 95°C, 2 min; 95°C, 10 s and 60°C, 45 s for 40 cycles; and 60°C for 71 cycles for a melt curve.

Table S2. Effect of compound 1 on IC_{50s} and EC_{50s} of proteins in various signaling pathway of PDAC cells

Signaling Pathway	Protein Marker	Cell Lines[a]	IC_{50}, EC_{50} ± SD, nM[b]
Activation of DNA Damage Checkpoint	Phospho-S1981-ATM	MIA PaCa-2	10 ± 4
	Up-regulated	HPAC	24 ± 6
		BxPC-3	16 ± 5
	Phospho-S428-ATR	LM-P	9.3 ± 1.3
	Up-regulated	MIA PaCa-2	8.2 ± 4.1
		HPAC	43 ± 11
p53 activation (total protein level)	p53	LM-P	25 ± 11
	Up-regulated	HPAC	30 ± 10
	Phospho-S15-p53	LM-P	8.9 ± 3.5
	Up-regulated		
	Phospho-S46-p53	HPAC	108 ± 27
	Up-regulated		
Apoptosis Activation	Bcl-xL	MIA PaCa-2	26 ± 3
	Inhibition	BxPC-3	46 ± 13
		779E	11 ± 3
	PARP cleavage	MIA PaCa-2	21 ± 3
	Up-regulated	BxPC-3	29 ± 9
Microtubule Destabilization	Acetylated-Tubulin	LM-P	94 ± 45
	Inhibition	MIA PaCa-2	81 ± 37
		HPAC	71 ± 15
		BxPC-3	236 ± 37
		AsPC-1	257 ± 35

[a]Cell lines were commercially available from ATCC except two cell lines: LM-P, isolated from the liver of KrasG12D/+; LSL-Trp53R172H/+; Pdx-1Cre mice; 779E: patient-derived, low passage primary PDAC cell lines (Dr. Andrew Lowy, UCSD). [b]Values were EC_{50s} except Bcl-xL, Acetylated-Tubulin inhibition, which were IC_{50s}. The data was presented as mean ± standard deviation (SD) and accurate values of full range concentrations (at least 5-point dilutions) of 2-3 replicates.

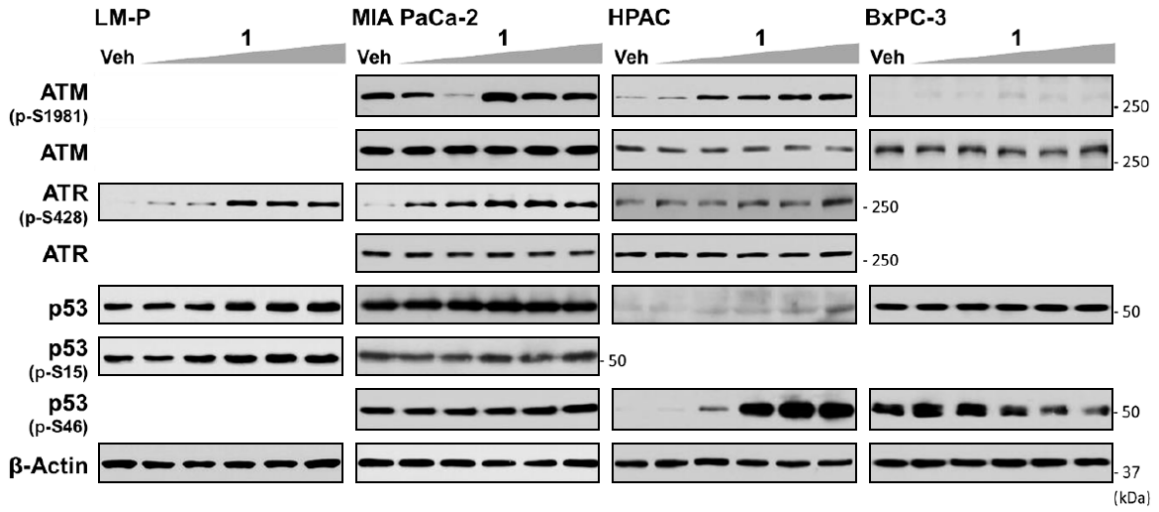

Figure S1. Dose-response for compound 1 on protein markers of DNA damage and p53 activation: phospho(Ser1981)-ATM, total ATM, phospho(Ser428)-ATR, total ATR, total p53, phospho(Ser15)-p53 and phospho(Ser46)-p53 as determined from whole-cell extracts of LM-P, MIA PaCa-2, HPAC and BxPC-3 cells following 4 h treatment. The concentration of 1 was 1.6, 8, 40, 200 and 1000 nM for LM-P, MIA PaCa-2 and BxPC-3 cells and 8, 40, 200, 1000, 2000 nM for HPAC cells. Veh, vehicle control (0.5% DMSO). A total of 25 μg of whole-cell protein extract was loaded into each lane. β-Actin was used as an internal control.

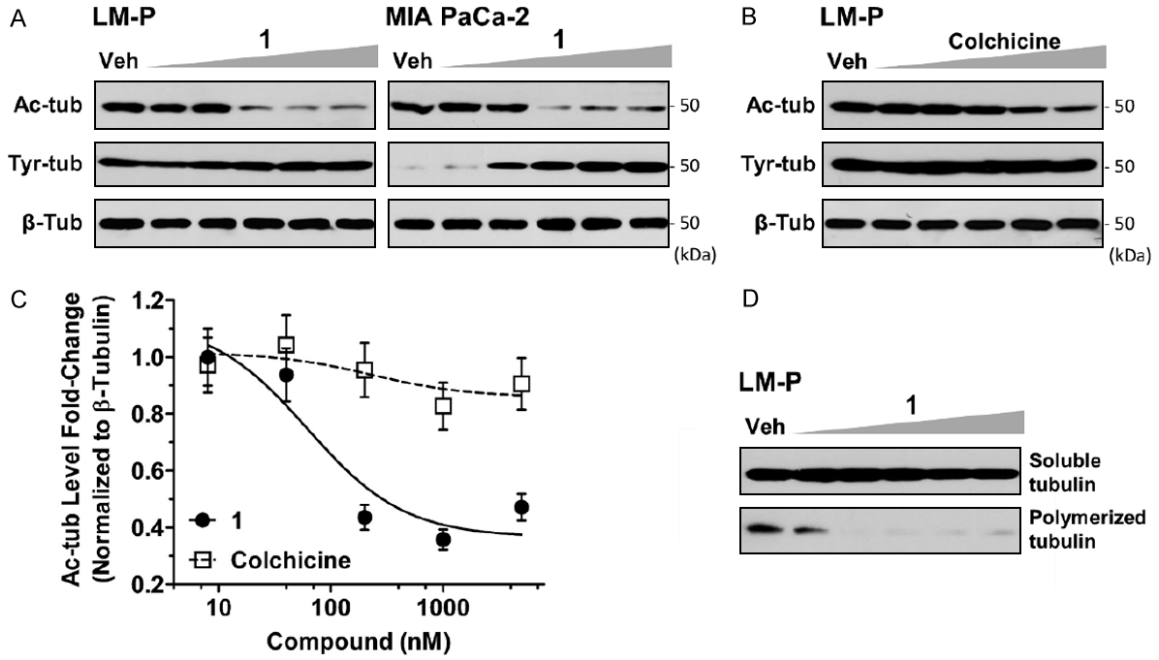

Figure S2. Western blot analysis of (A) 1 or (B) colchicine on acetylated-, tyrosinated- or β-tubulin as determined from whole-cell extracts of LM-P and MIA PaCa-2 cells following 4 h treatment. (C) The effect of 1 (solid circle) and colchicine (open square) on inhibition of acetylated-tubulin protein levels (normalized to β-tubulin) in LM-P cells by densitometry analysis of (B and C). (D) Effect of 1 on cellular soluble and polymerized tubulin levels in LM-P cells. The concentration of 1 or colchicine in (A, B and D) were 8, 40, 200, 1000 and 5000 nM; Veh, vehicle control (0.5% DMSO). A total of 25 μg of whole-cell extracted protein (A, B) or 10 μg of subcellular extracted protein (D) was loaded into each lane. Data are mean ± SD (n=3) in (C).

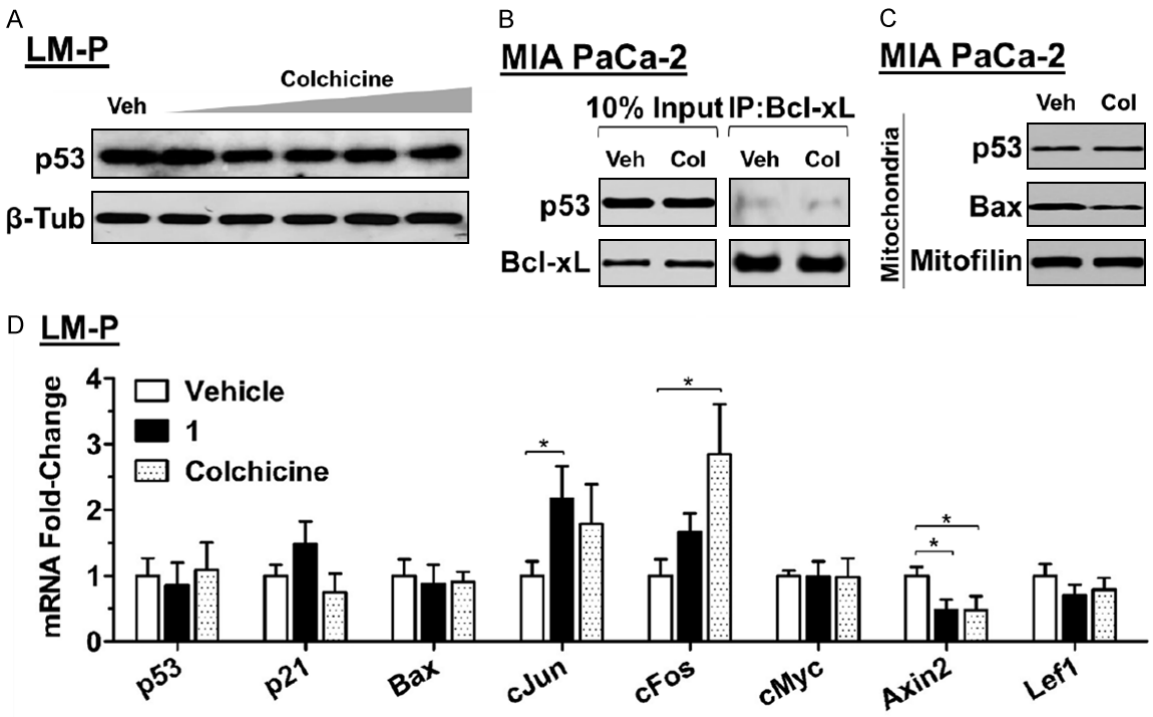

Figure S3. Effect of colchicine on (A) total p53 (p53) and total tubulin (β-Tub) in whole-cell extracts of LM-P cells following 4 h treatment with colchicine (i.e., 8, 40, 200, 1000 or 5000 nM); (B) immunoprecipitation of p53 and Bcl-xL in the cytoplasmic extract of MIA PaCa-2 cells and (C) p53 and Bax levels in mitochondrial extracts of MIA PaCa-2 cells following 4 h treatment with colchicine (200 nM). β-tubulin was used as a cytoplasmic extract control and mitofilin was used as a mitochondria marker. Veh, vehicle control (0.5% DMSO); Col, colchicine; p53, total p53; β-Tub, total tubulin. (D) The effect of 1 or colchicine on the regulation of apoptotic and Wnt target gene expression in LM-P cells. White bar, vehicle control (0.5% DMSO)-treated LM-P cells; black bar, 1 (500 nM)-treated LM-P cells; hatched bar, colchicine (500 nM)-treated LM-P cells. Data represent the mean ± SD of relative mRNA determined for compound-treated cells relative to vehicle control. *P*-values were estimated with a Student's *t*-test (**P*<0.05).

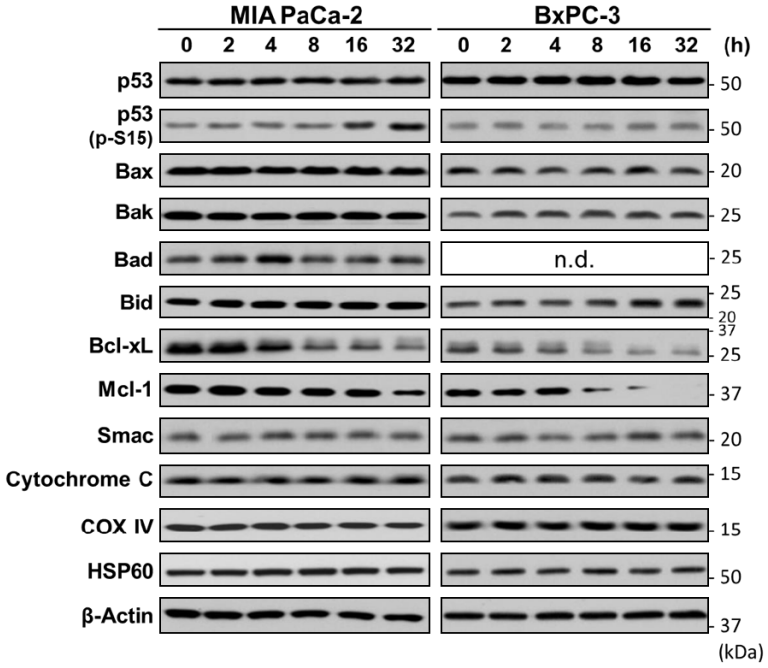

Figure S4. Time-dependent response for compound 1 on protein markers for p53-dependent apoptosis: total p53, phospho(Ser15)-p53, Bax, Bak, Bad, Bid, Bcl-xL, Mcl-1, Smac, Cytochrome C, COX IV, HSP60 as determined from whole-cell extracts of MIA PaCa-2 and BxPC-3 cells following 0-32 h treatment. The concentration of 1 was 50 nM. A total of 25 μg of whole-cell extracted protein was loaded into each lane. β-Actin was used as an internal control; n.d., not detected.

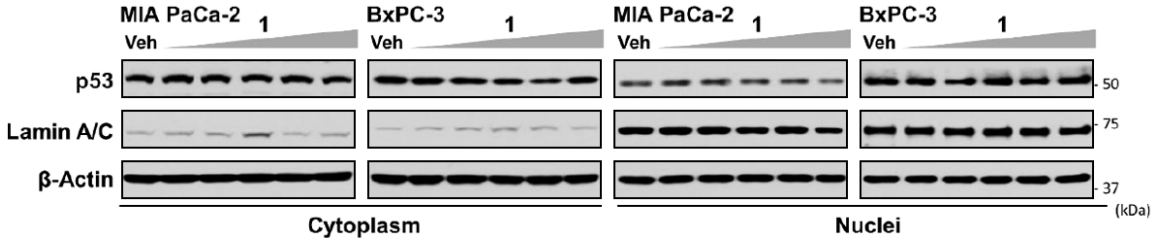

Figure S5. Dose-response for compound 1 on cytoplasmic and nuclear p53 accumulation of p53 in MIA PaCa-2 and BxPC-3 cells following 4 h treatment. The concentration of 1 was 1.6, 8, 40, 200 and 1000 nM. Veh, vehicle control (0.5% DMSO). A total of 25 μg of protein extract was loaded into each lane. β-Actin was used as internal control. Lamin A/C was used as a marker of the nuclear fraction.

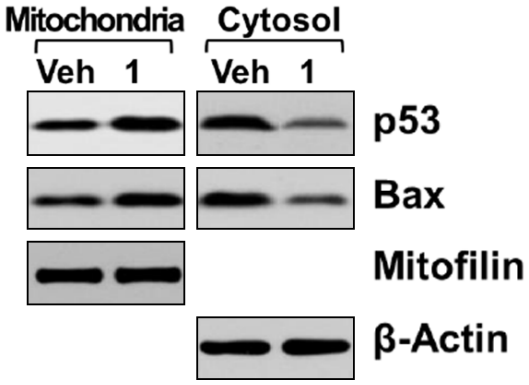

Figure S6. Effect of compound 1 on p53 and Bax levels in mitochondrial and cytosolic extracts of HPAC cells following 8 h treatment. Veh, vehicle control (0.5% DMSO); 1, 50 nM. β-Actin was used as a cytosolic extract control and mitofilin was used as a mitochondria marker.

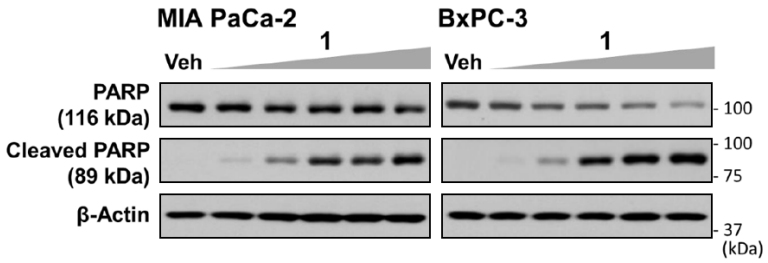

Figure S7. Dose-response for compound 1 on PARP cleavage as determined with whole-cell extracts of MIA PaCa-2 and BxPC-3 cells following 24 h treatment. The concentration of 1 was 15, 20, 35, 50 and 100 nM. Veh, vehicle control (0.5% DMSO). A total of 25 μg of whole-cell extract protein was loaded into each lane. β-Actin was used as internal control.

Table S3. Effect of paclitaxel or gemcitabine on PDAC cell proliferation

Cell Line	Gemcitabine[a] IC_{50} ± SD, nM (*N*)[b]	Paclitaxel[c] IC_{50} ± SD, nM (*N*)[b]
LM-P	10 ± 2 (*3*)	8.6 ± 1.3 (*3*)
MIA PaCa-2	26 ± 5 (*3*)	2.3 ± 1.2 (*3*)
HPAC	17 ± 3 (*4*)	4.1 ± 0.9 (*4*)
BxPC-3	7.3 ± 2.6 (*4*)	1.3 ± 0.4 (*4*)
AsPC-1	22 ± 10 (*4*)	3.1 ± 1.9 (*4*)
779E	31 ± 2 (*3*)	2.1 ± 1.8 (*3*)
1334E	5.5 ± 1.2 (*3*)	6.6 ± 1.7 (*3*)

[a]Gemcitabine-treated dose-range was 1.6-5,000 nM. [b]IC_{50} was the mean ± standard deviation (SD) of 3-4 independent determinations. (*N*) represents the replicate number. [c]Paclitaxel-treated dose-range was 0.3-1,000 nM.

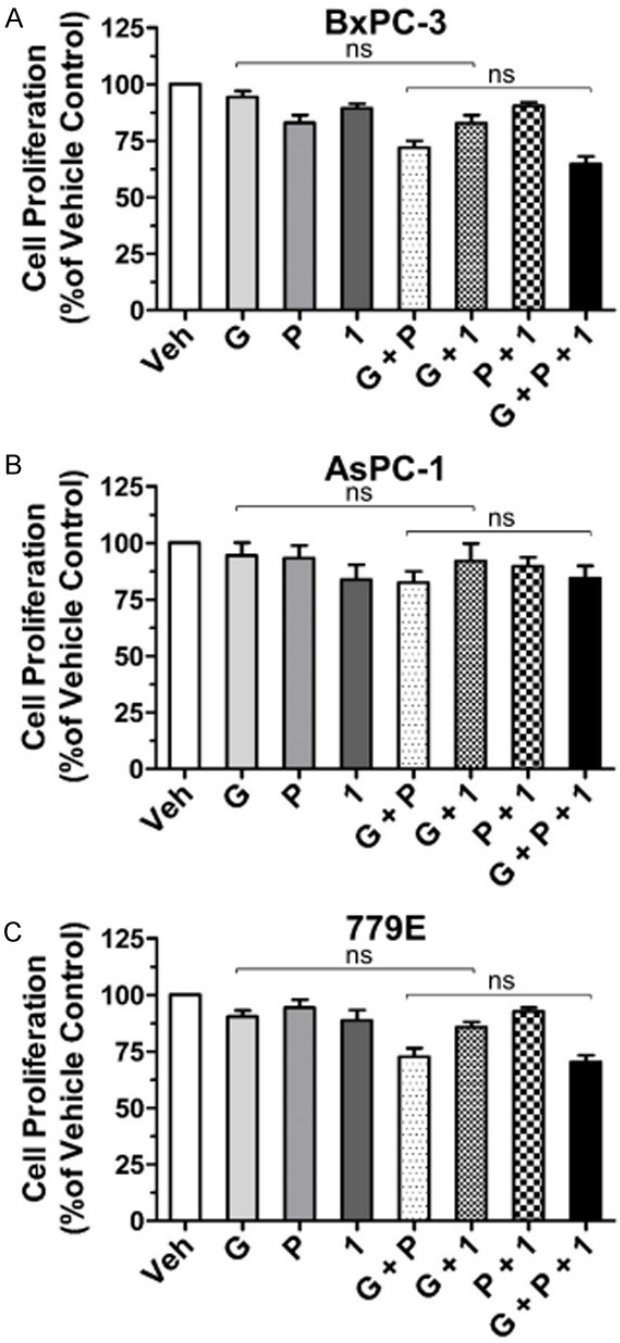

Figure S8. Effect of gemcitabine (G, 2-8 nM) and/or paclitaxel (P, 1 nM) in the presence of 1 (4-8 nM) on PDAC cell proliferation among cell types. (A) BxPC-3 (1, 4 nM; P, 1 nM; G, 4 nM); (B) AsPC-1 (1, 8 nM; P, 1 nM; G, 8 nM); and (C) 779E (1, 4 nM; P, 1 nM; G, 4 nM). Data represent the mean ± SD (n=3) of percent cell proliferation determined for compound-treated cells relative to vehicle-treated cells. Veh, vehicle control (0.5% DMSO); P, paclitaxel; and G, gemcitabine. The *P*-value was determined by Student's *t*-test (ns = no significant difference).

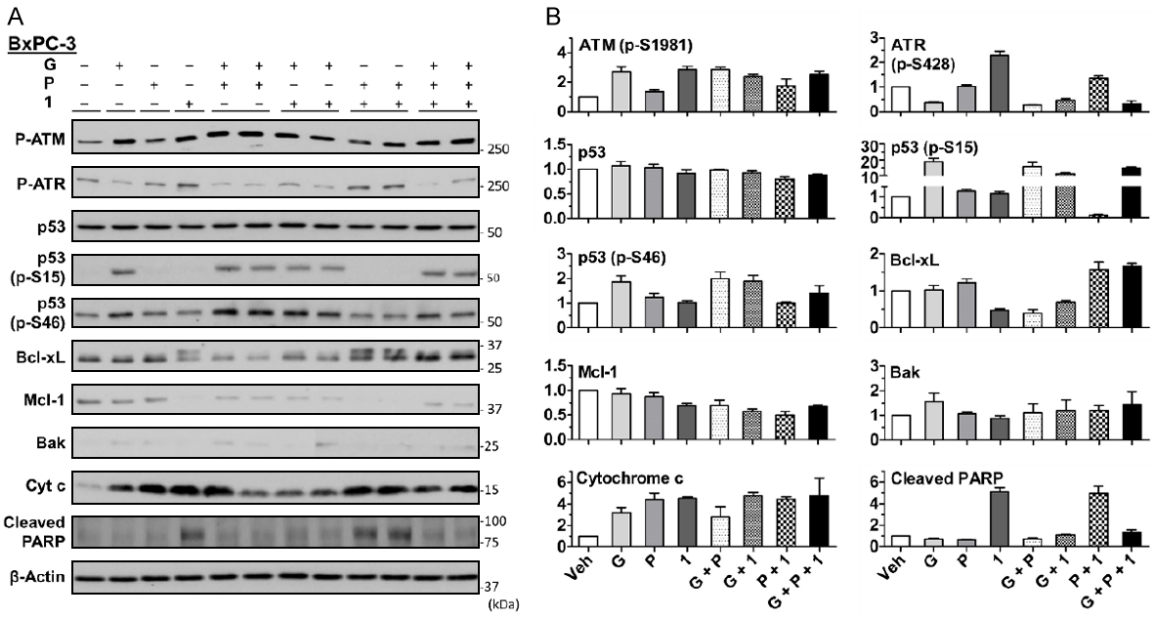

Figure S9. (A) Western blot and (B) densitometry analysis for the combination of gemcitabine (G, 50 nM) and/or paclitaxel (P, 5 nM) in the presence of 1 (50 nM) on phospho(Ser1981)-ATM, phospho(Ser428)-ATR, p53, phospho(Ser15)-p53, phospho(Ser46)-p53, Bcl-xL, Mcl-1, Bak, Cytochrome C and cleaved PARP as determined from whole-cell extract of BxPC-3 cells. Treatment time was 16 h. β-Actin was used as an internal control. Data represents mean ± SD (n=3) of protein level fold-changes in (B) as determined for compound-treated samples relative to vehicle control. Veh, vehicle control (0.5% DMSO); P, paclitaxel; and G, gemcitabine.

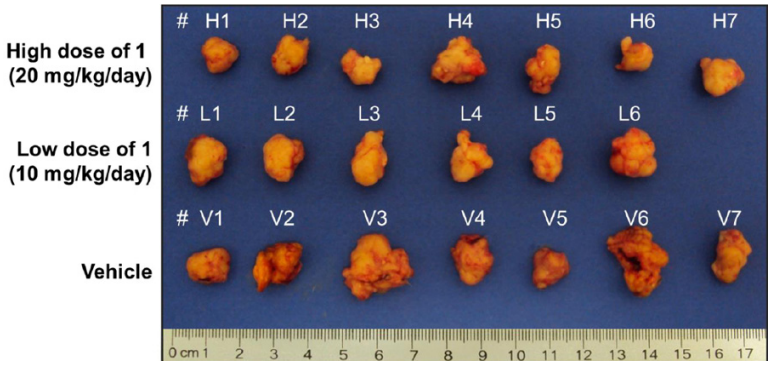

Figure S10. Excised mouse LM-P cell tumors from an orthotopic study conducted for 28 days in mice. Top row, tumors from high-dose of 1-treated animals (20 mg/kg/day, i.p., n=7, #H1-H7); middle row, tumors from low-dose of 1-treated animals (10 mg/kg/day, i.p., n=6, #L1-L6); bottom row, tumors from vehicle-treated animals (aqueous-DMSO-Captisol, i.p., n=7, #V1-V7).

Table S4. Clinical chemistry serum values observed for vehicle- and compound 1-treated mice

Condition	Parameter (mean ± SD)[a]							
	ALP[b] (U/L)	SGPT (ALT)[b] (U/L)	SGOT (AST)[b] (U/L)	Albumin (g/dL)	BUN[b] (mg/dL)	Creatinine (mg/dL)	Cholesterol (mg/dL)	Glucose (mg/dL)
1	73 ± 16	32 ± 7	609 ± 44	1.8 ± 0.0	72 ± 57	<0.3[c]	64 ± 18	76 ± 46
Vehicle	32 ± 8	34 ± 23	850 ± 180	1.8 ± 0.3	59 ± 35	<0.3[c]	44 ± 21	38 ± 13

[a]Mean and standard deviation (SD) of independent analysis of serum samples from three high dose-treated animals (20 mg/kg/day of 1 for 28 days, i.p.) and three vehicle-treated animals (aqueous-DMSO-Captisol). [b]ALP: Alkaline Phosphatase; SGPT (ALT): Serum Glutamic Pyruvic Transaminase (Alanine Aminotransferase); SGOT (AST): Serum Glutamic OxaloaceticTransaminase (Aspartate Aminotransferase); BUN: Blood Urea Nitrogen. [c]The result was obtained by dilution of the original serum samples.

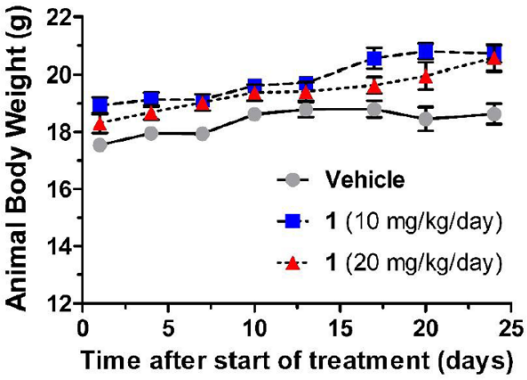

Figure S11. Average orthotopic mice body weight (g) of the groups treated with vehicle or two different doses of 1 (daily, 28 days, i.p.). Body weights were monitored twice a week after the initial injection of treatment. Circle, vehicle (aqueous-DMSO-captisol), n=7; Square, 10 mg/kg/day of 1, n=6; triangle, 20 mg/kg/day of 1, n=7. Data are mean ± SEM.

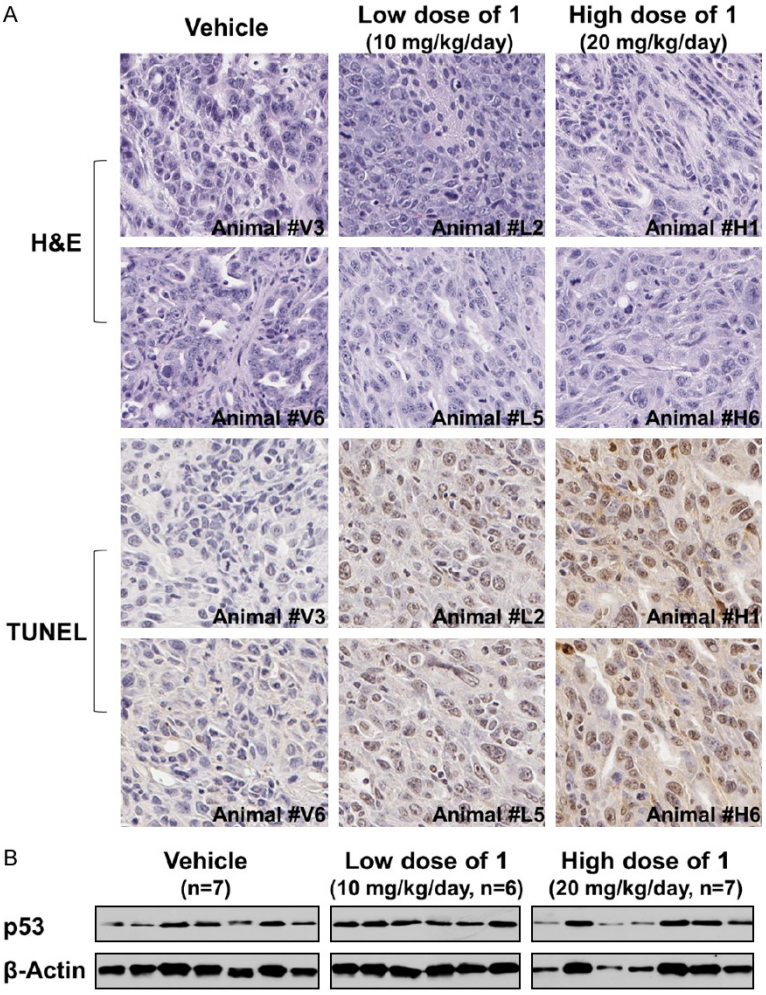

Figure S12. A. Representative photographs of tumor sections (original magnification, × 550) of animals (as shown in Figure S10) by H&E and TUNEL staining. Brown staining indicates TUNEL-positive nuclei and blue staining counterstained with hematoxylin indicates TUNEL-negative nuclei; B. Western blot analysis of compound 1 on total p53 and β-actin in vehicle- (aqueous-DMSO-captisol, i.p., n=7), low-dose (10 mg/kg/day of 1 for 28 days, i.p., n=6) and high-dose (20 mg/kg/day of 1 for 28 days, i.p., n=7)-treated tumors excised from mice tissue on day 29 of the study.

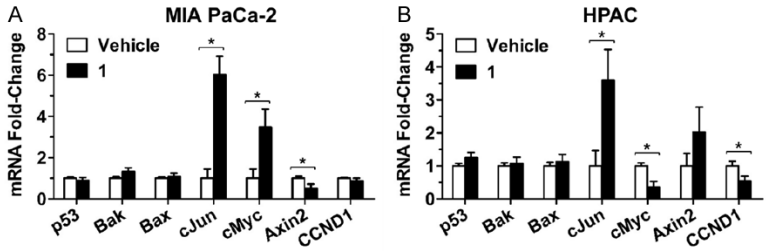

Figure S13. Effect of 1 on apoptotic and Wnt target gene expression in (A) MIA PaCa-2 and (B) HPAC cells. Black bar, 1-treated cells (i.e., 500 nM, 4 h); and white bar, vehicle control (0.5% DMSO)-treated cells. Data represent the mean ± SD (n=4) of relative mRNA determined for compound-treated cells relative to vehicle control. The *P*-value was determined by Student's *t*-test (**P*<0.05).

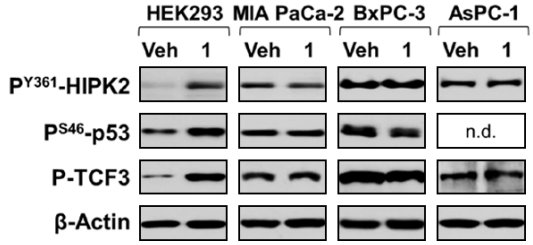

Figure S14. Effect of 1 on phospho-HIPK2, phospho(Ser46)-p53, phospho-TCF3 protein levels from total protein extracts of HEK293 (WT p53), MIA PaCa-2 (Arg248Trp p53), BxPC-3 (Tyr220Cys p53) and AsPC-1 (135Δ1bp p53, like -/-p53) cells and analyzed by Western blot. The treatment was 40 nM of 1 for 4 h; Veh, vehicle control (0.5% DMSO). β-Actin was used as internal control; n.d., not detected.